NASA/CR- 1998 207486

FINAL REPORT: Contract #: **NAS8-39926**

TITLE: **ADVANCED HIGH BRILLIANCE X-RAY SOURCE**

Principal Investigator: Walter M. Gibson
Center for X-Ray Optics
University at Albany
Albany, NY 12222

Section I. INTRODUCTION

In a joint effort between the center for X-Ray Optics (CXO) at the University at Albany, State University of New York and the Laboratory for Structural Biology at NASA Marshall Space Flight Center (MSFC), the possibility to dramatically increase the efficiency of laboratory based protein structure measurements through the use of polycapillary x-ray optics was investigated. This project initiated April 1, 1993 and concluded December 31, 1996 (including a no cost extension from June 31, 1996). This is a final report of the project.

The basis for the project is the ability to collect x-rays from divergent electron bombardment laboratory x-ray sources and redirect them into quasiparallel or convergent (focused) beams. For example, a 0.1 radian (~6°) portion of a divergent beam collected by a polycapillary collimator and transformed into a quasiparallel beam of 3 millradian (0.2°) could give a gain of $6^2/0.2^2$ x T for the intensity of a diffracted beam from a crystal with a 0.2° diffraction width. T is the transmission efficiency of the polycapillary diffraction optic, and for T=0.5, the gain would be 36/0.04x0.5=45. In practice, the effective collection angle will depend on the source spot size, the input focal length of the optic (usually limited by the source spot-to-window distance on the x-ray tube) and

the size of the crystal relative to the output diameter of the optic. The transmission efficiency, T, depends on the characteristics (fractional open area, surface roughness, shape and channel diameter) of the polycapillary optic and is typically in the range 0.2-0.4. These effects could substantially reduce the expected efficiency gain.

During the course of this study, the possibility to use a weakly focused beam (0.5^{o} convergence) was suggested which could give an additional 10-20 X efficiency gain for small samples . Weakly focused beams from double focusing mirrors are frequently used for macromolecular crystallography studies. Furthermore the crystals are typically oscillated by as much as 2^{o} during each x-ray exposure in order to increase the reciprocal space (number of crystal planes) sampled and use of a slightly convergent beam could, in principle, provide a similar sampling benefit without oscillation. Although more problematic, because of complications in analyzing the diffraction patterns, it was also suggested that even more extreme beam convergence might be used to give another order of magnitude intensity gain and even smaller focused spot size which could make it possible to study smaller protein crystals than can be studied using standard laboratory based x-ray diffraction systems. This project represents the first systematic investigation of these possibilities.

As initially proposed, the contract included requirements for design, purchase, evaluation and delivery of three polycapillary lenses to the Laboratory for Structural Biology at MSFC and demonstration of such optics at MSFC for selected protein crystal diffraction applications. These deliverables were:

> Stage I. Collimating optic <50 mm input focal distance, 5 mm output diameter, >0.1 radian capture angle, >0.2 transmission efficiency. <20μm output channel diameter, <4.0 mrad divergence. Goal: to provide an output x-ray intensity through a 0.3 mm collimator equal to or better than that available through a comparable collimator from the existing rotating

anode-graphite monochrometer system at the Laboratory for Structural Biology at MSFC.

Stage II. Collimating optic. <30 mm input focal distance, 3 mm output diameter, >0.1 radian capture angle, >0.2 transmission efficiency, <15 μm output channel diameter, <4.0 mrad divergence. Goal: to provide an output x-ray intensity 10 X or higher through a 0.3 mm collimator relative to that available through a comparable collimator from the same source at 250 mm from the source.

Stage III. Collimating optic. <5 mm input focal distance, 1 mm output diameter, >0.2 radian capture angle, >0.2 transmission efficiency, <10 μm output channel diameter, <4.0 mrad divergence. Goal: to provide an output x-ray intensity 100 X or higher through a 0.3 mm collimator relative to that available through a comparable collimator at the same source at 250 mm from the source (it was recognized that the shorter focal distance of this optic would preclude use of the existing rotating anode source without modification and therefore a special close-coupling microfocus source would need to be purchased).

The stage I optic was designed to be used with a rotating anode x-ray generator at MSFC which was to be fitted with a 0.2 x 2.0 mm spot size on the anode. The input focal distance of 50 mm was chosen to be compatible with the anode-window distance on the MSFC Ragaku RU 300 rotating anode x-ray generator including the beam shutter. It was felt that the Stage II optic could be accommodated by modification of the rotating anode by use of a re-entrant window and use of a cathode filament which would give a 0.1x100 anode spot size. The Stage III optic would require a new x-ray generator designed to give improved access (5 mm) and a smaller (50 μm x 500 μm) spot size.

After preliminary measurements and discussions between MSFC, XOS and CXO personnel and approval from the NASA Program Officer, the deliverables were modified as follows:

Stage I. The same as the initially proposed Stage I optic.

Stage II. A weakly focusing optic (convergence angle ~0.5°), <50 mm input focal distance, 100 mm output focal distance, ~ 0.1 radian capture angle, Goal unchanged.

Stage III. A strongly focusing optic (convergence angle ~2°), 30 mm input focal distance (chosen to allow use of an existing tube based microfocus x-ray source), 25 mm output focal distance, ~ 0.1 radian capture angle Goal unchanged.

A prototype Stage I optic was provided by X-Ray Optical Systems, Inc. (XOS) (designated Stage IA). Although this optic did not meet all of the design criteria indicated above, it gave benefit which already exceeded the Stage I goal (to equal or exceed the x-ray intensity and measurement efficiency of the standard protein x-ray crystallography system in use at MSFC). This optic was subsequently replaced by XOS (at no extra cost) with an optimized Stage I optic. The parameters and performance of this optic will be discussed in Section IIIA. The parameters and performance of the Stage II (or weakly focusing) optic and the Stage III (strongly focusing) optic are discussed in Section IIIB and IIIC, respectively.

Presentations and publications are discussed in Section IV and the project summary and future plans are given in Section V.

A special microfocus x-ray source was purchased from X-Ray Optical Systems, Inc. for evaluation and characterization of the prototype x-ray optics indicated above. This source, produced in Viborg, Russia was developed for x-ray microscopy and has the ability to produce a highly focused, adjustable, x-ray spot (5-50 μm) on a water cooled anode which is at ground potential and which can be rotated (not continuously) to expose fresh target material or to change the target material without breaking vacuum. Also the Beryllium exit window is very close to the target anode which allowed close coupling between the polycapillary optic and the x-ray source spot (as close as 2 mm).

Section II. GENERAL PRINCIPLES AND DESIGN PARAMETERS

A. General Principles

Polycapillary optics is based on the fact that x-rays undergo efficient total external reflection from solid surfaces at grazing angles of incidence. A plot of the reflectivity of 6 and 8 keV x-rays from a smooth borosilicate glass surface is shown in Fig. 1. For a given x-ray energy and solid density, the reflection is close to unity for angles below a critical angle, θ_C, and drops rapidly for angles above θ_C. The critical angle, θ_C, is inversely proportional to the x-ray energy and depends on the electron density of the scattering surface. For borosilicate glass, the critical angle, $\theta_C = 30/E_X$ where θ_C is in milliradians (mr) and the x-ray energy, E_X, is in keV. Using this effect, it is possible to transport x-rays through hollow glass capillary tubes as shown in Fig. 2 and to deflect the x-rays by gently bending the hollow capillary as shown in Fig. 3 such that at each reflection the incident angle is less than the critical angle for the x-ray energy and the particular material involved. The efficiency for such transmission is governed by a dimensionless quantity γ which is given by

$$\gamma = \theta_C^2/\theta^2 = R\theta_C^2/2d \qquad \text{(eq. 1)}$$

where R is the bending radius of the capillary tube and d is the diameter of the tube. For γ equal to 1 or greater, the entire tube will transmit efficiently but as γ decreases below 1, the transmission becomes increasingly less efficient. It is clear from eq. 1 that as the bending radius, R, decreases (as required for compact optics) or as the x-ray energy increases (smaller θ_C), the diameter of the capillary tube, d, must decrease. For the applications considered in this report, typical values of d needed will be in the range from 10-20 μm.

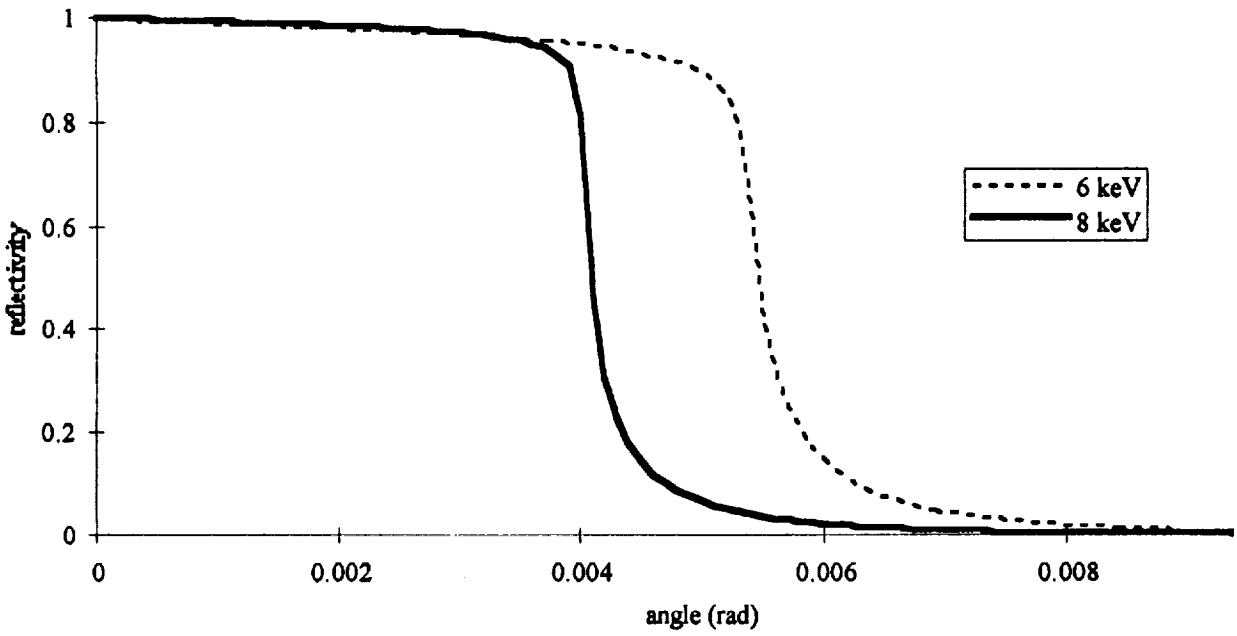

Figure 1. Reflectivity vs. angle for 6 keV (dotted line) and 8 keV (solid line). x-rays reflected from borosilicate glass. The critical angles, θ_c, are 5.5 and 4 mrad. respectively.

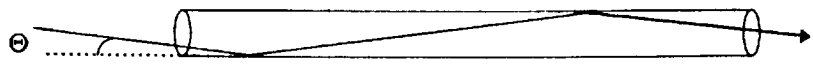

Figure 2. Photon being transported through a hollow glass capillary by total external reflection.

Figure 3. Propagation of an x-ray through a bent capillary

Because of the small diameters, using individual capillaries is precluded because of their flexibility and fragility. Therefore, many such hollow capillaries are combined into a single glass polycapillary fiber as shown in Fig. 4. As many as 2000 such capillary channels can be contained in a single fiber of diameter about 0.5 mm.

For the monolithic optics developed for the program reported here, hundreds of such fibers were combined and the resulting bundle was shaped to produce a "lens" as shown schematically in Fig. 5 which shows important design parameters; f, the focal distance; ω, the collection angle; L, the length;, d, the input diameter; D, the output diameter; and; Θ, the local x-ray beam divergence from each capillary channel.

B. Single Fiber Measurements

Before attempting to construct any of the lenses to be studied in this program it was necessary to carry out measurements with a large number of straight and bent polycapillary fibers. In order to do this it was necessary to develop new measurement techniques. For example, the technique used to bend the fibers in a controlled and reproducible way is shown in Fig. 6. Measurements of transmission efficiency and, beam divergence, for a large number of fibers were carried out. In addition, analytical and computer simulation ray tracing techniques were developed to provide a basis for interpreting the results and to aid in the design and evaluation of monolithic optics. An example of such measurements and calculations for a single bent fiber is shown in Fig. 7.

C. Optics Fabrication

Since this project was one of the first applications of the monolithic optics technology, it included development of many of the processes involved in the lens fabrication. The monolithic lenses were tapered in a setup shown schematically in

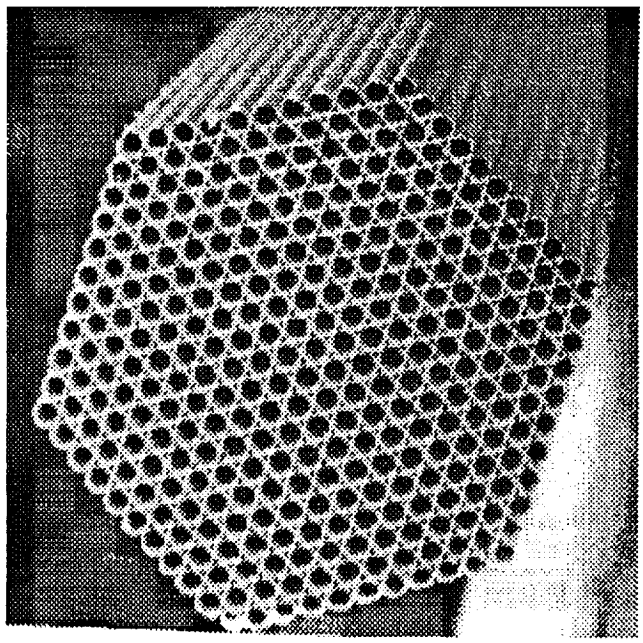

Figure 4. Electron micrograph of a cross-section of a polycapillary fiber. The width of the hollow hexagonal channels in this fiber is 15 μ m flat to flat.

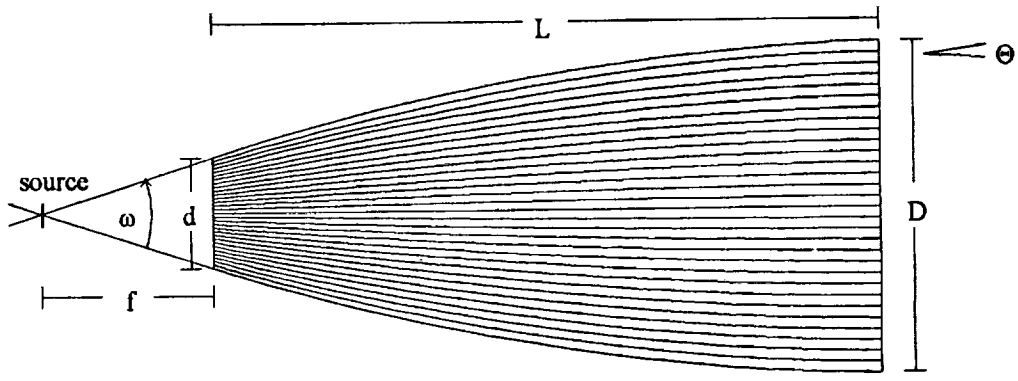

Figure 5. Schematic of a collimating monolithic optic.

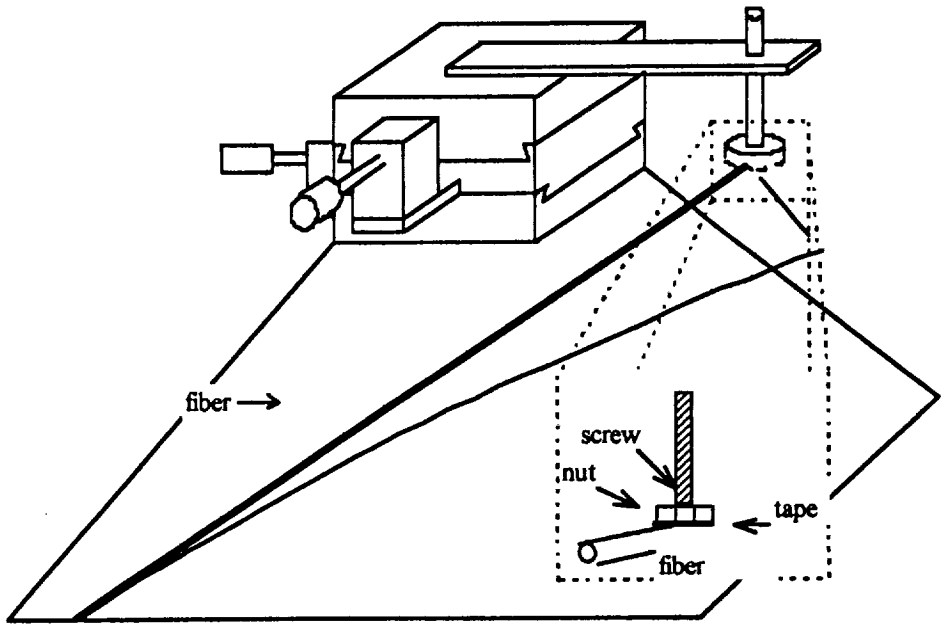

Figure 6. Setup for circularly bent fibers. The fiber is taped to the baseplate at one end and to a nut at the other end. The nut is hanging at the end of a screw so it can turn freely. The screw is moved by a precision x-y stage.

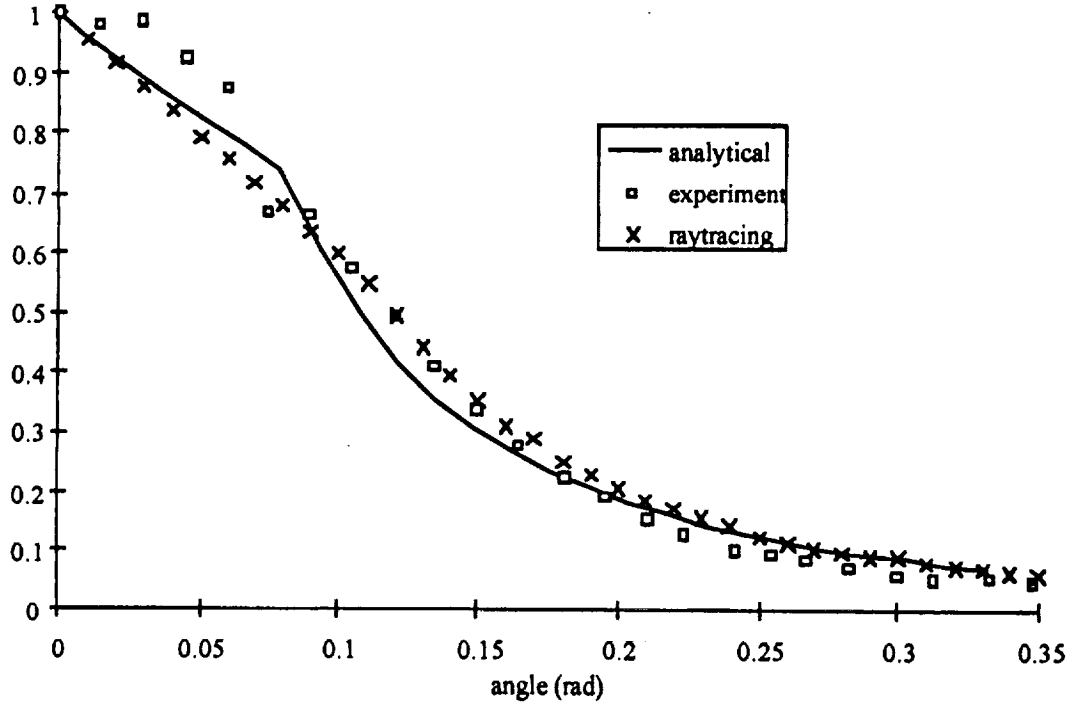

Figure 7. Analytical approximation and computer simulation (ray tracing) for a bent fiber compared to experimental transmission measurements. The measurements and calculations are normalized for the no bending case. The average reflectivity used for the calculations is 0.985.

Fig. 8. This setup used two motors to move both ends of the fiber billet (assembly of 100-200 polycapillary fibers). A portion of the billet was heated by a furnace. After the billet was heated to the working temperature the taper was pulled at a predetermined rate. Since a number of different parameters had to be taken into account, a computer model was developed to predict the outcomes of a number of different pulling modes. This model is based on a one dimensional finite differences algorithm. The model takes radiative heating by the furnace into account as well as radiative cooling. The geometry of the furnace with some of the parameters used in the calculation is shown in Fig. 9 The viscosity and specific heat for borosilicate glass as a function of temperature were approximated by semiemperical expressions taken from the literature.

The final shape of the monolithic collimating optics were first measured by measuring the diameter with a vernier gauge. This turned out to be totally inadequate in terms of precision or accuracy. Therefore, a long focus traveling microscope coupled to a video camera was obtained by XOS. This is shown schematically on Fig. 10. The profile (radius) measured for one of the first "successful" optics as measured by this system is shown on Fig. 11 compared to a best fit assuming a circular profile. If the profile were truly circular, the curvature and therefore the second derivative should be constant. That this is not the case is clearly shown in Fig. 12 and Fig. 13. This optic also exhibited a lower transmission than predicted by simulations assuming a circular profile but agreed better with simulations in which the measured profile was used. In addition, the optic showed imperfect bonding of capillary fibers near the edge as shown in Fig. 14 by a micrograph taken with x-rays transmitting through the optic. A great deal of effort was spent to determine the origin of the apparent "waviness" that appeared to reduce the transmission of this optic. That this effort was successful will be evident from results that will be discussed section III.

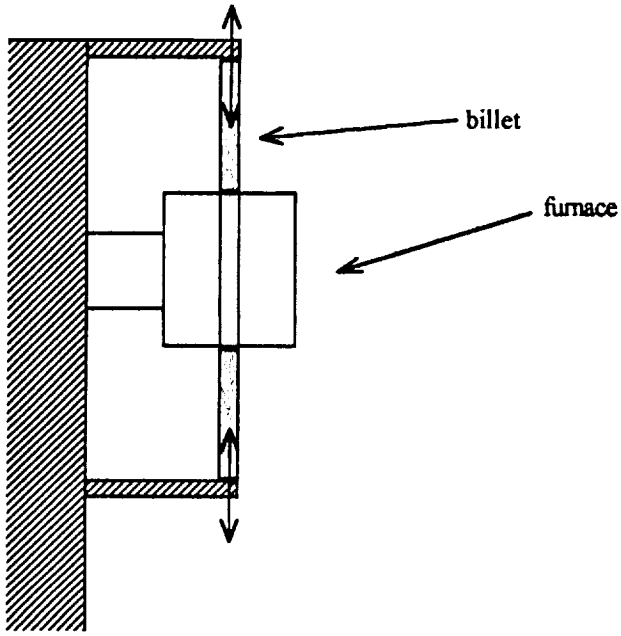

Figure 8. Sketch of taper pulling setup.

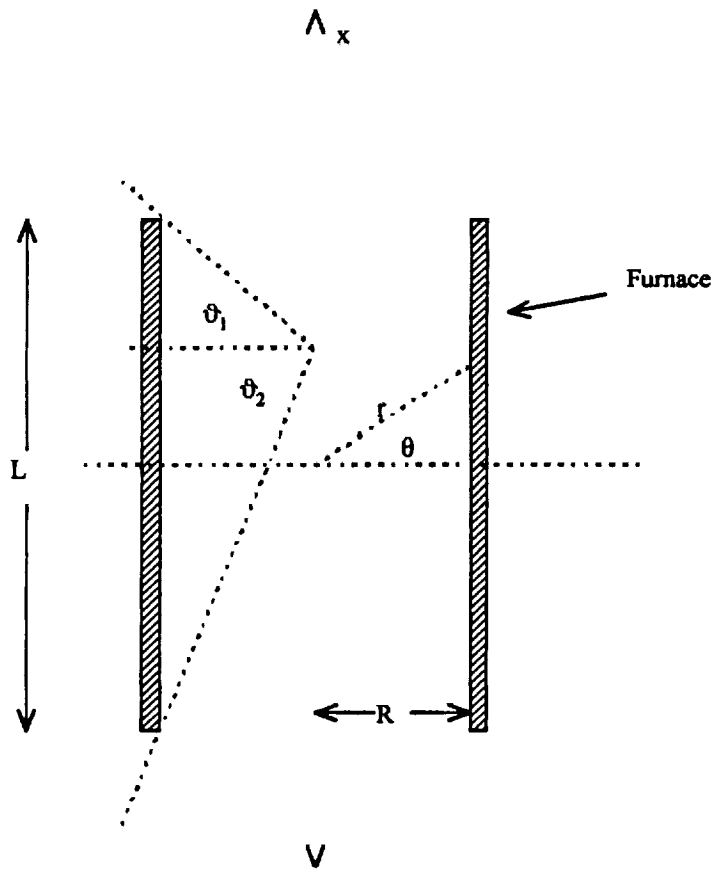

Figure 9. Sketch of furnace geometry.

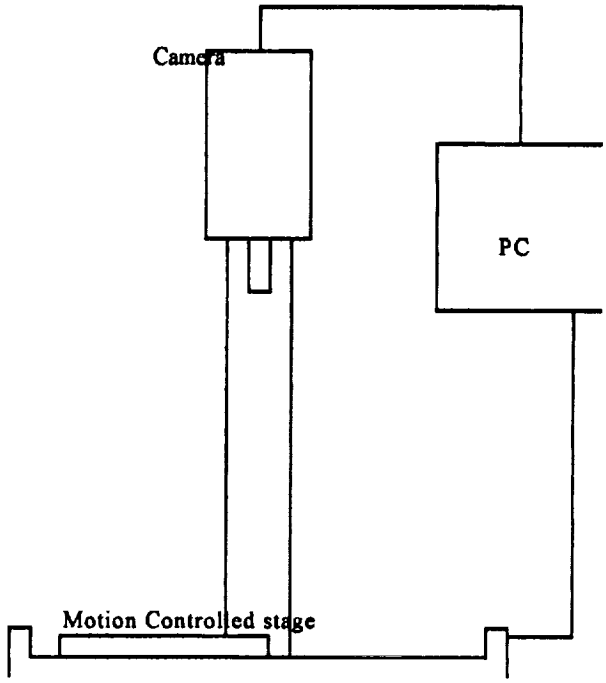

Figure 10. Sketch of the microscope system used to measure lens profiles.

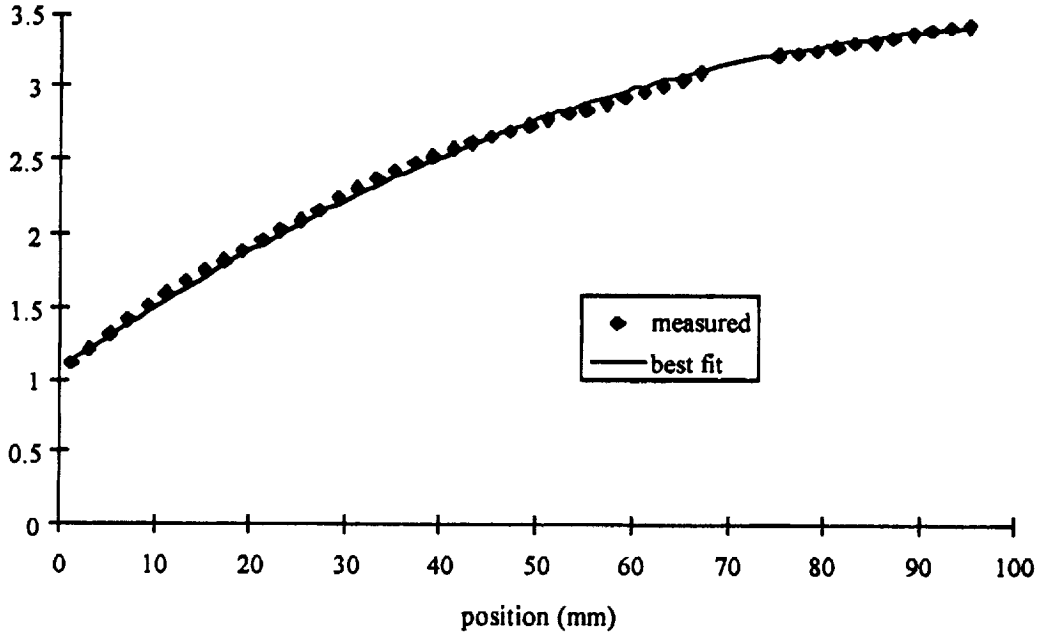

Figure 11. Measured radius of lens 5.5.2 and best fit to circular profile.

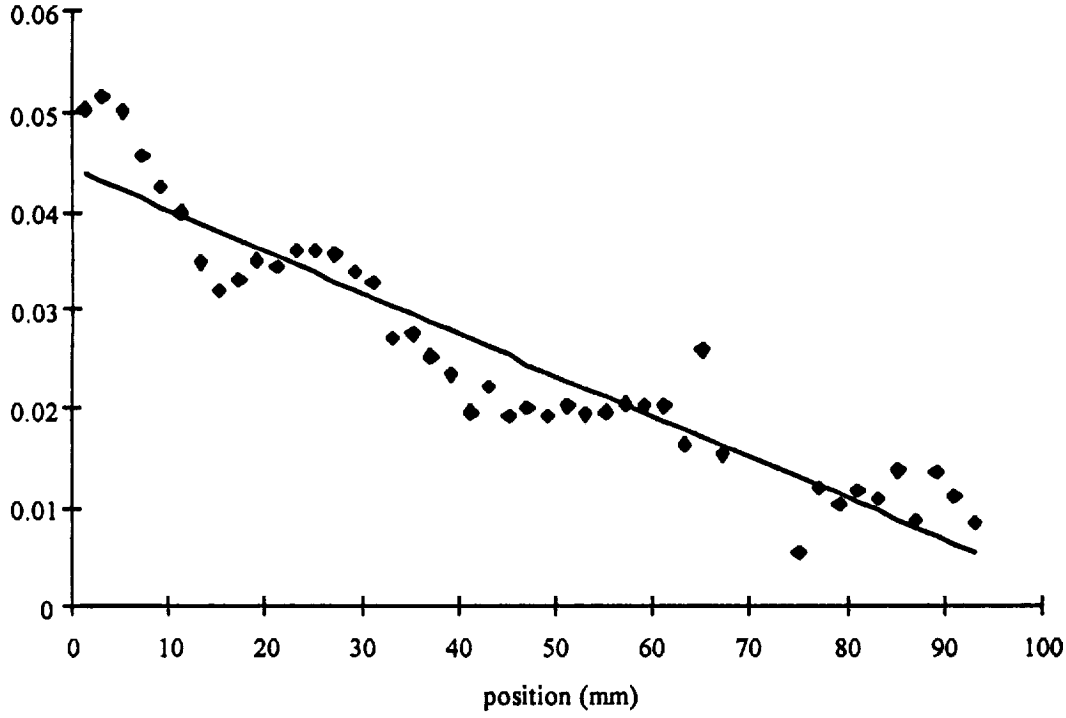

Figure 12. Derivative of the radius of lens 5.5.2 and linear best fit.

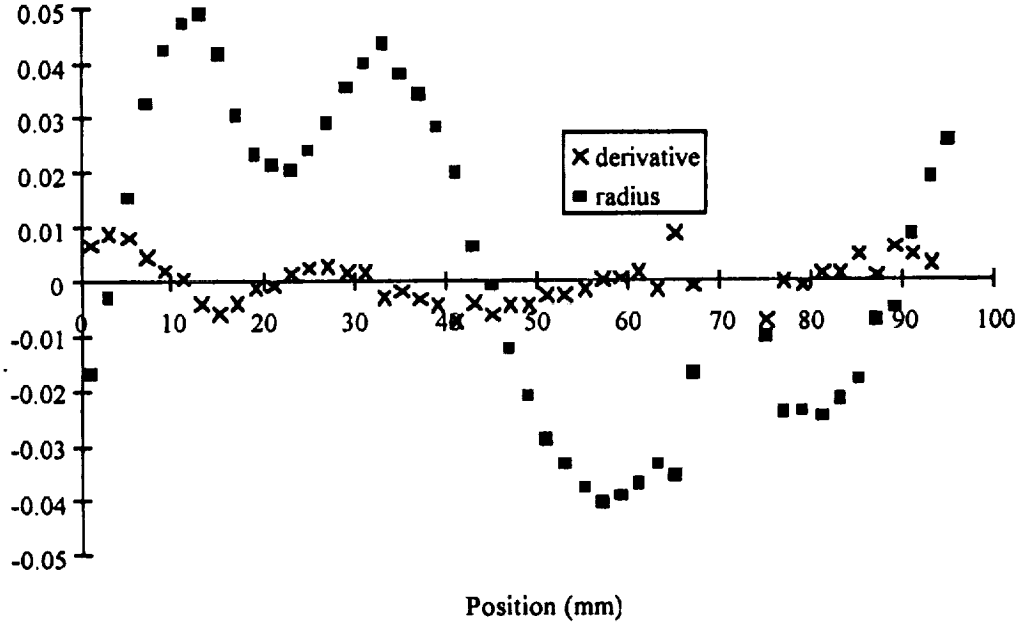

Figure 13. Residuals for radius and derivative fit for lens 5.5.2.

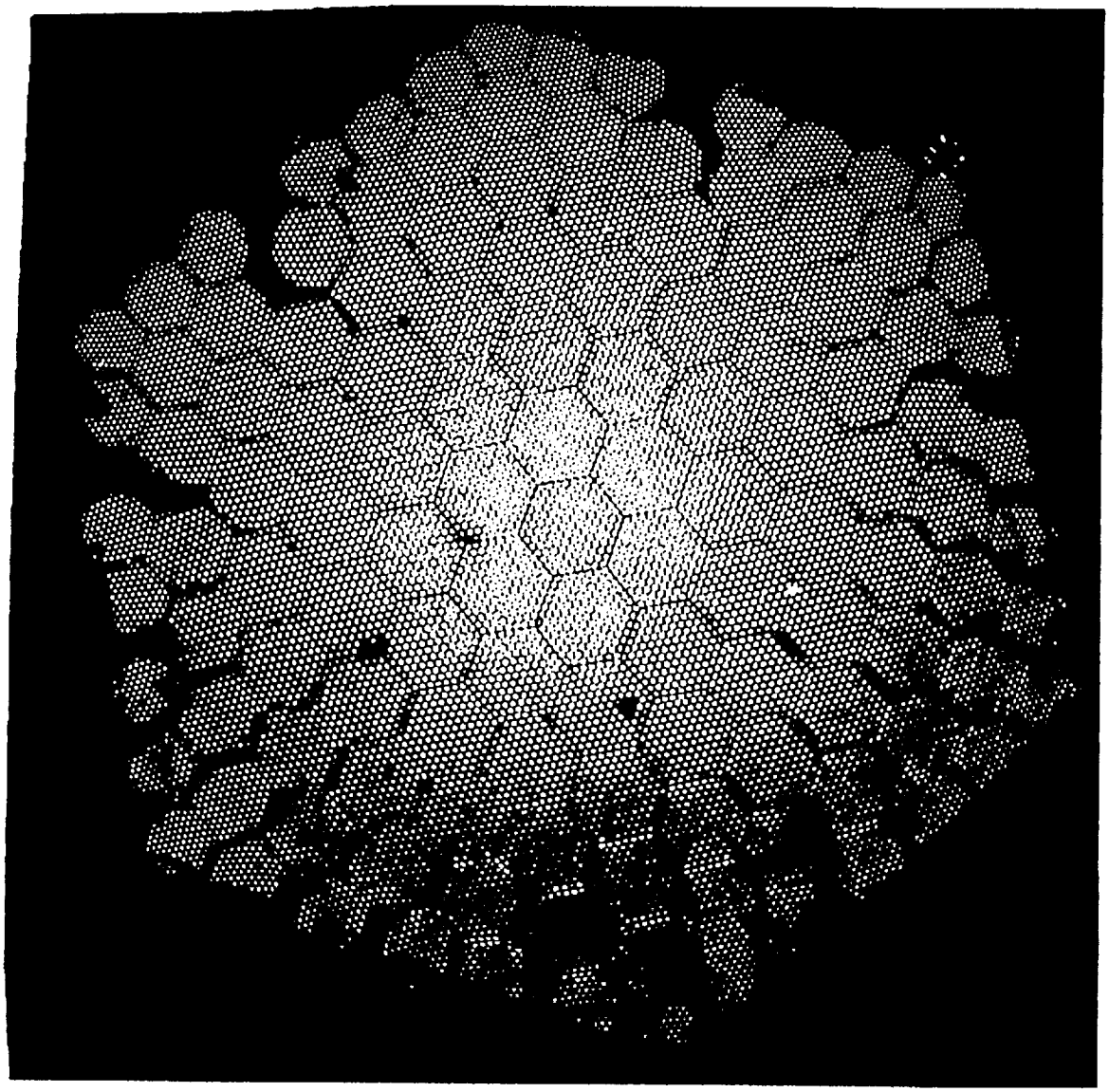

Figure 14. X-Ray micrograph (made by transmitted x-rays) of lens 5.5.2.

In addition to the profile, it was necessary to determine fabrication conditions to control the fractional open area at the input of the optic. Even an optic with a perfect profile could have the channels close up at the input, reducing the open area. The transmission cannot exceed the open area at the input of the optic. In addition, optics with a significantly different fractional open area at the input compared to the output of the optic, invalidates the assumption of a self aligned system and leads to defocusing or unnecessarily strongly bent outer channels. Furthermore, it was necessary to maintain a very high surface smoothness on the interior of the channels (rms. roughness of not more than 2-3 Angstroms). Altogether, more than two dozen optics were fabricated and tested in identifying and evaluating the complex, multiparameter fabrication processes involved in producing the high quality monolithic optics needed for this project. Although this went far beyond the scope and support of this project, it was ultimately successful and laid the groundwork for subsequent development of controlled, reproducible monolithic optics fabrication.

A system was developed for systematic transmission measurements. This is shown in Fig. 15. The best of a series of prototype collimating optics (labeled lens 1945) was characterized extensively at CXO and subsequently taken to MSFC in Huntsville for the initial protein crystallography measurements. The profile for this optic as measured with the traveling microscope-video system is shown on Fig. 16 and transmission measurements for 8 keV Cu Kα radiation as a function of the x-ray source position relative to the center line of the optic are shown for the entire 5 mm diameter optic in Fig. 17 and for the central 3.5 mm in Fig. 18. These results show that the outer channels continue to be less well aligned but, when compared to the computer simulation, show that the transmission efficiency is within 3/4 of that expected.

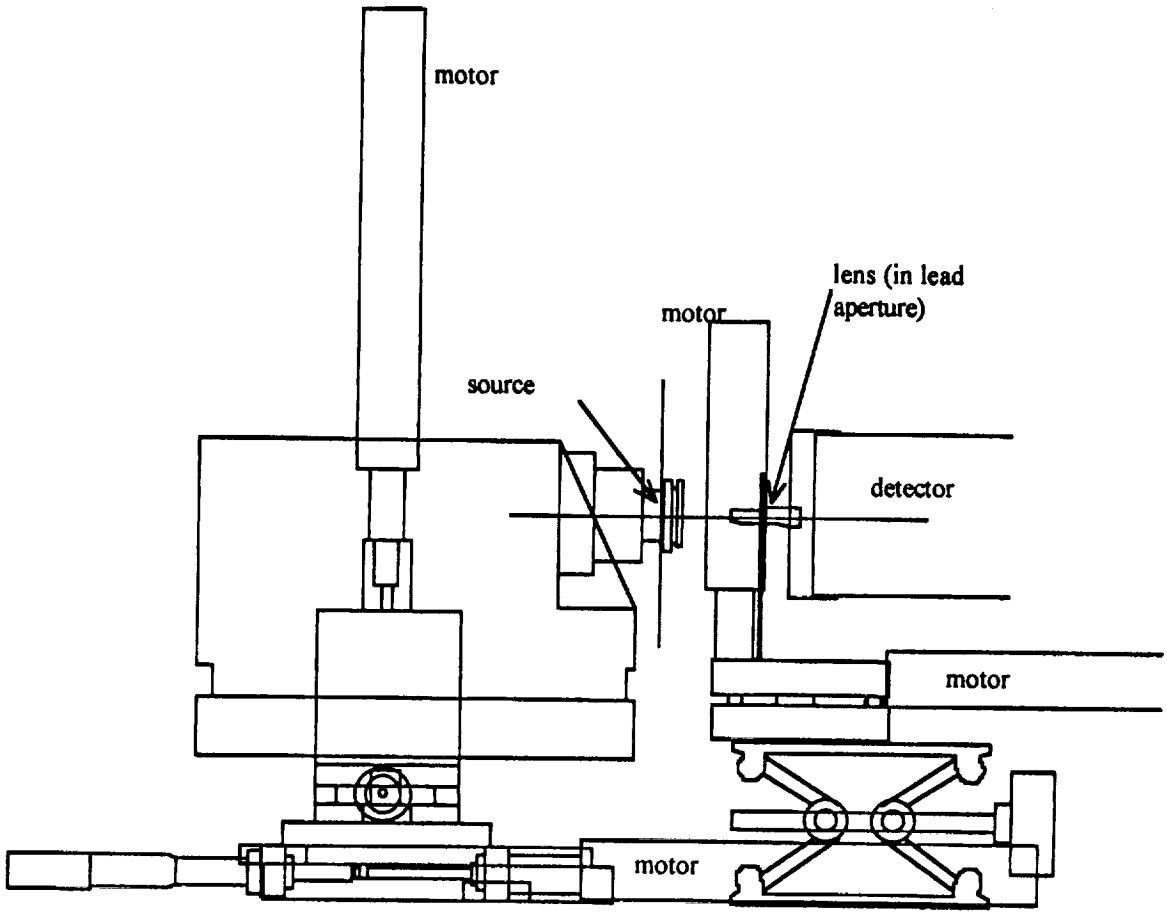

Figure 15. Sketch of the setup used for transmission measurements for monolithic optics.

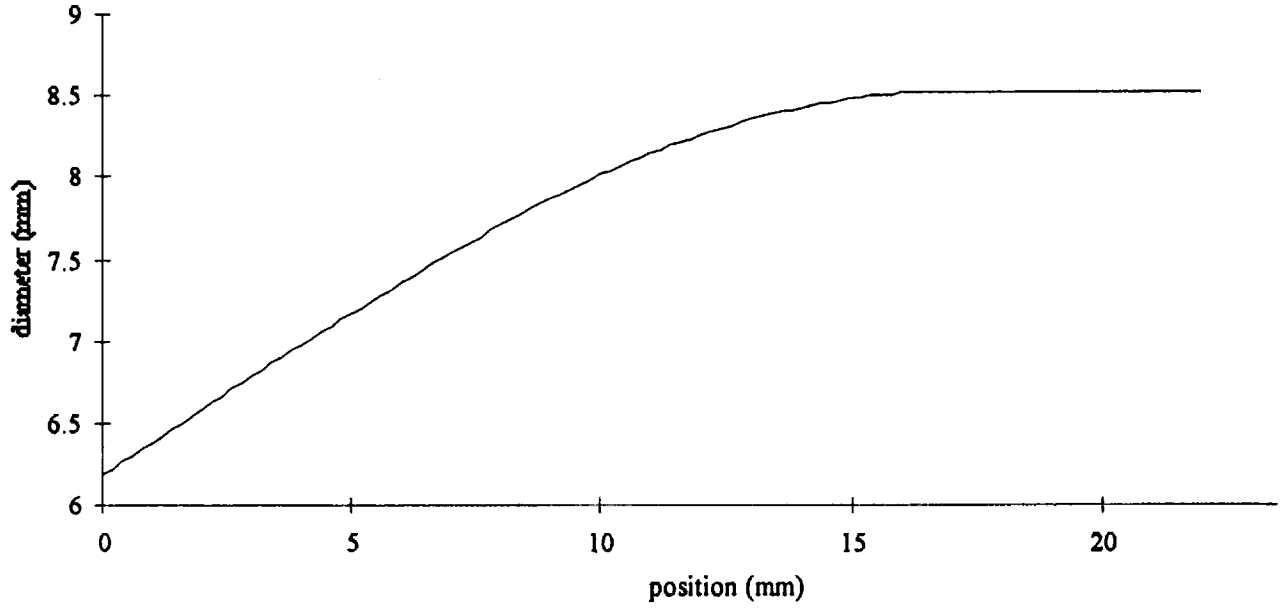

Figure 16. Shape of lens 1945 (data) (Stage IA optic)

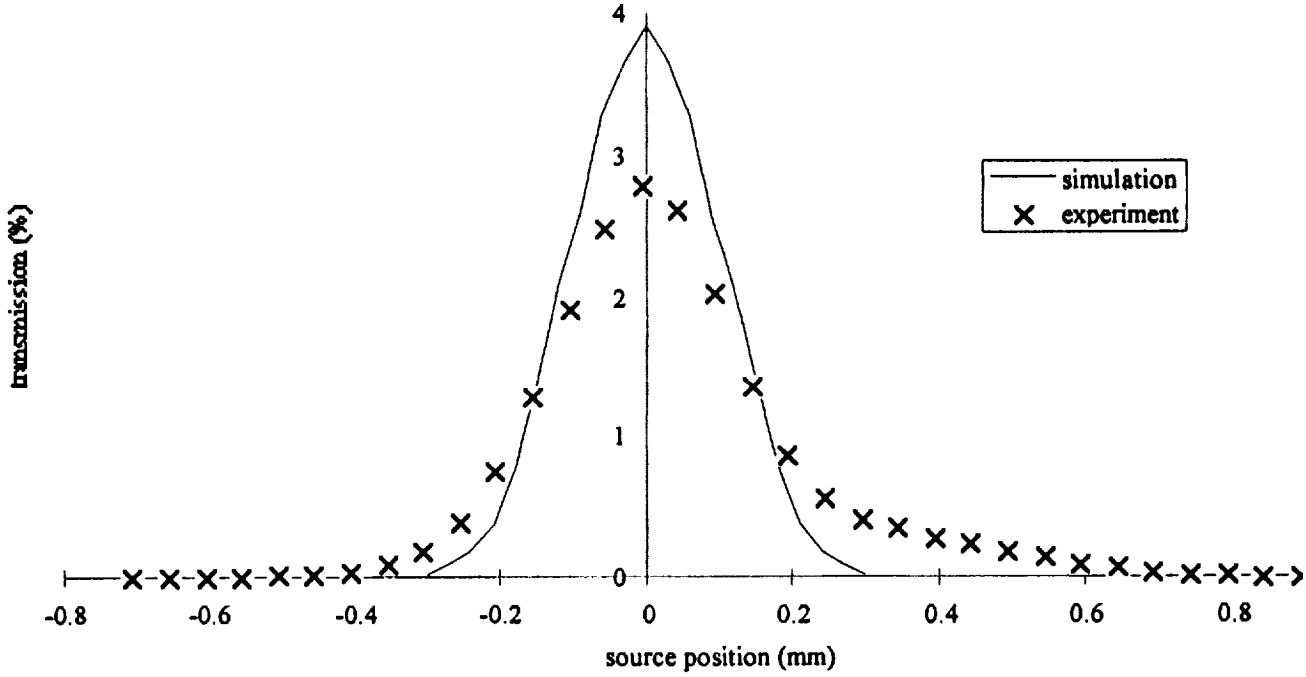

Figure 17. Measured and simulated transmission of lens 1945 for different source positions.

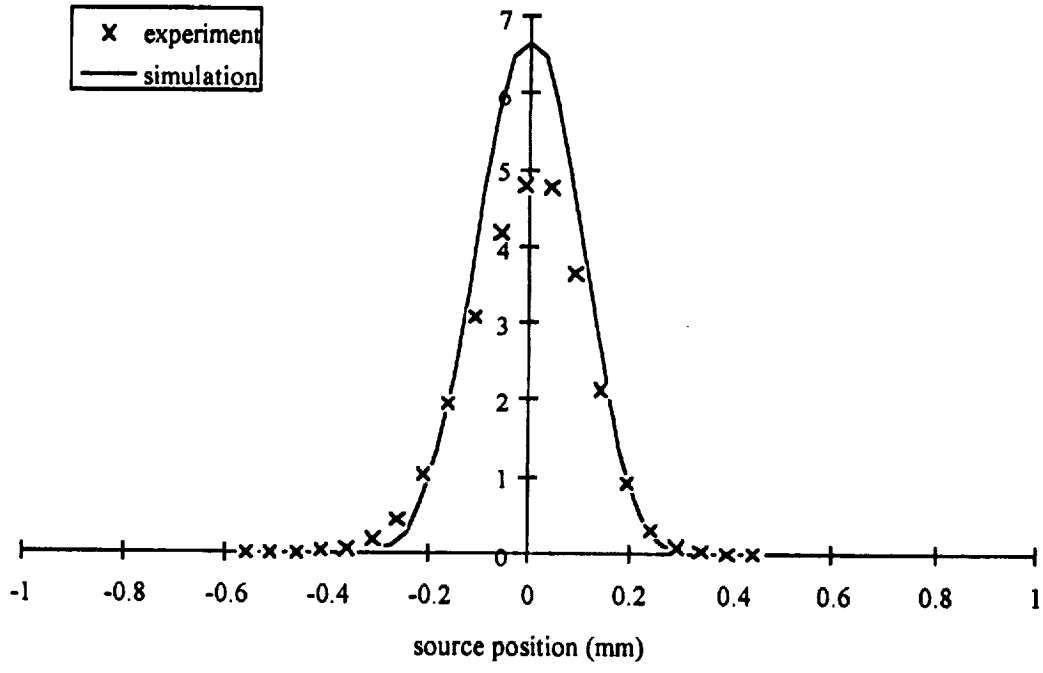

Figure 18. Measured and simulated transmission for different source positions for the inner 3.5 mm of lens 1945.

This optic was used for initial measurements at MSFC, and easily met the goal for Stage I. This optic was called Stage IA and produced the first exciting diffraction patterns and provided the initial experience with integration of the optics into a working protein crystallography system. This integration included development of alignment, shielding, and collimation apparatus and procedures. This work formed the basis for the first publications. Based on the studies at CXO and XOS in Albany and at MSFC in Huntsville, improvements were made in the fabrication, mounting, shielding, and collimation of the optic and in the crystal mounting, system alignment and data collection procedures. These were all incorporated into the measurements reported in Section III.

D. Source Development.

As originally planned, the ultimate optic for protein crystallography was to be a collimating optic with a 1 mm output diameter and a 0.1-0.2 radian collection angle. Liouville's theorem which applies to all optics and derives from the second law of thermodynamics places important constraints on the nature of the x-ray source and on the coupling of the source and optic for such a collimating optic. Liouville's theorem can be expressed in a variety of ways, but for these optics, the most applicable is the form:

$$L\Omega = l\omega \qquad \text{(eq. 2)}$$

L gives the size of the object before the optic, and Ω is the divergence at the same point. The size of the image at the other end of the optic is given by l and ω is the divergence at that point. In order to achieve a perfectly parallel beam at the output, it is necessary to use an ideal point source at the input end. For a real system, the source size must be considerably smaller than the output size of the lens in order to achieve a useful gain. A beam size of 1 mm was planned for the original Stage III optic The output divergence is usually found to be close to the

critical angle, which for 8 keV x-rays is about 4 mrad. To collect x-rays over and angle of 0.1 rad, the source diameter must be smaller than 40 μm. Furthermore, the input of the optic will need to be less than 5 mm. For a collection angle of 0.2 rad a source size of 20μ and source-lens distance of 2.5 mm is required. Since these conditions were not met by any of the sources usually employed for protein crystallography are even any of the available commercial microfocus sources, it was necessary to locate and purchase the most appropriate source that could be found.

Other considerations include the reduction in total x-ray power as the source size is reduced. This is because of a limitation of the temperature the source anode can endure before serious erosion by evaporation. The situation was analyzed by solution of both convective and radiative heat flow giving the result shown in Fig. 19 for a circular spot on a Copper anode. In the region of interest, a close approximation is about one watt per μm. Water cooling, electron beam scanning or anode movement and use of line focus (viewed at a small take off angle) can in principle increase the total power. Following a systematic investigation it was learned that an x-ray source developed in Russia for electron microscopy apparently had many of the desired characteristics. Following two visits to Viborg, Russia where the source was manufactured, it was decided to purchase one of these sources. This microfocus x-ray generator has a special electron beam geometry which is shown schematically in Fig. 20. The cathode is far away from the anode. This allows an electromagnetic lens to focus the electron beam on the target. Electrons emitted by a filament are focused onto a tungsten foil by a Wehnelt cylinder. Electrons are emitted from the heated spot. This spot is then imaged on the anode by means of an electromagnetic lens. By purposely defocusing the electron beam by missaligning the lens, the spot size may be changed. Auxiliary coils also allow the beam shape to be changed. The

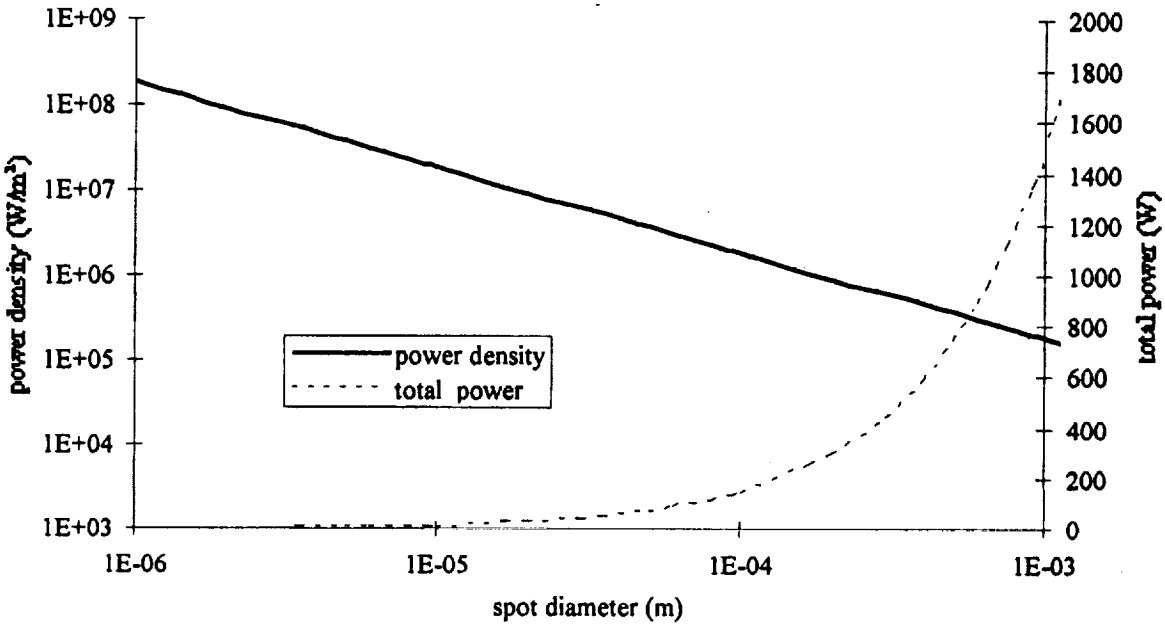

Figure 19. Calculated total power and power density for a 1 mm thick Cu anode x-ray source.

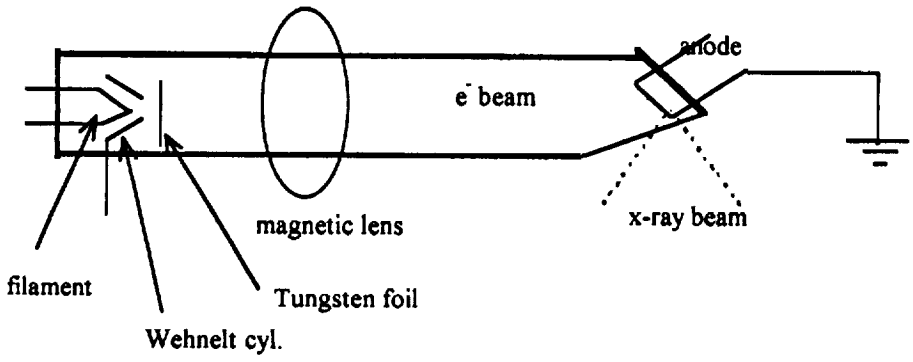

Figure 56: Schematic crossection of the electron gun.

Figure 20. Schematic cross section of the electron gun for the Viborg microfocus x-ray source.

electron beam strikes near the edge of the water cooled anode and close to the Be window, allowing close access by the optic. Using a copper target, a power of about 30 Watt could be achieved in a 5 μm spot. For higher power, the anode is damaged by the electron beam. The electron power density of this source is then 1.2×10^8 W/cm^2, compared to about 1.2×10^5 W/cm^2 for a typical rotating anode x-ray generator. A photograph of the anode area of the microfocus source is shown on Fig. 21

This Russian source proved to be difficult to use, much of the electronic system which controls the high voltage and beam focus needed to be replaced as well as the pumping system. As noted in the Introduction, the strategy for achieving high intensity and the design of the Stage II and Stage III optic was changed during the course of the project so building this special source into a protein crystallography system was not pursued. However, this special microfocus source has proved to be invaluable in characterizing monolithic optics for this and other projects.

Section III. RESULTS

In order to obtain high quality diffraction results, it is necessary to consider the spectral distribution of x-rays incident of the sample. Figure 22 shows the x-ray spectrum from a bare Cu source from a Ragaku RU 300 rotating anode x-ray generator operated at 37.5 keV with and without a polycapillary optic. Although the Stage II optic was used, similar results were obtained with the Stage I and the Stage III optic. The curves are normalized at the height of the Kα peak. It can be seen that the intensity of the Kβ peak is reduced and that higher energy bremstrahlung photons are almost completely suppressed by the optic. This is because of the energy dependence of the critical angle for x-ray reflection. The bare spectrum has 47.2 % of all photons in the Kα line, 12.4% in the Kβ line and

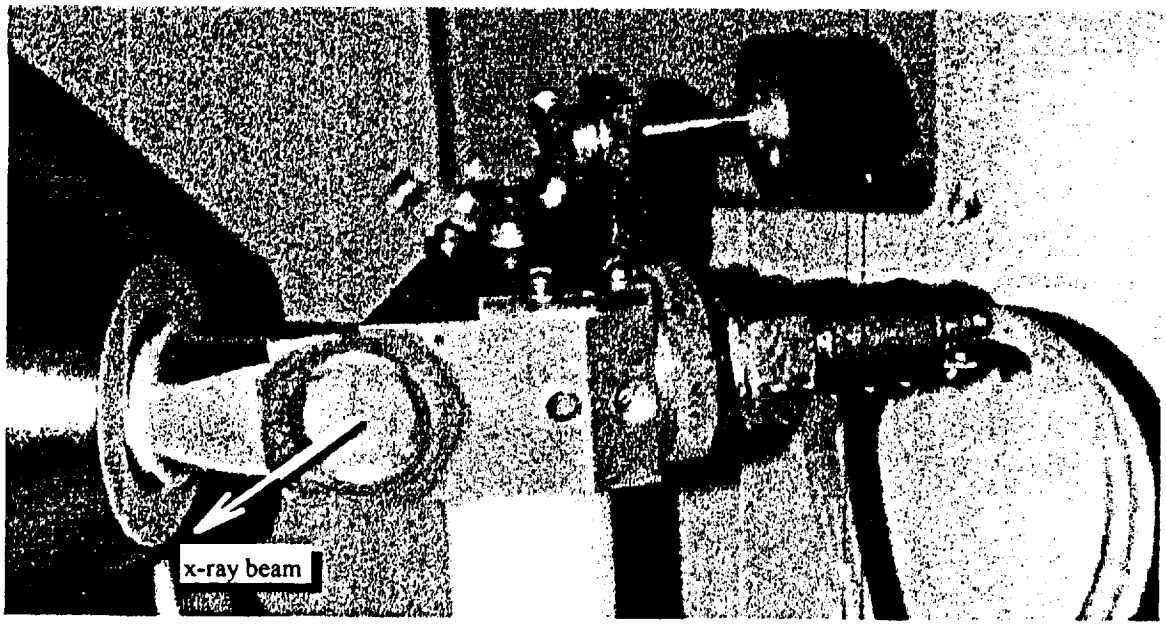

Figure 21. Photograph of the anode area of the Viborg microfocus x-ray source.

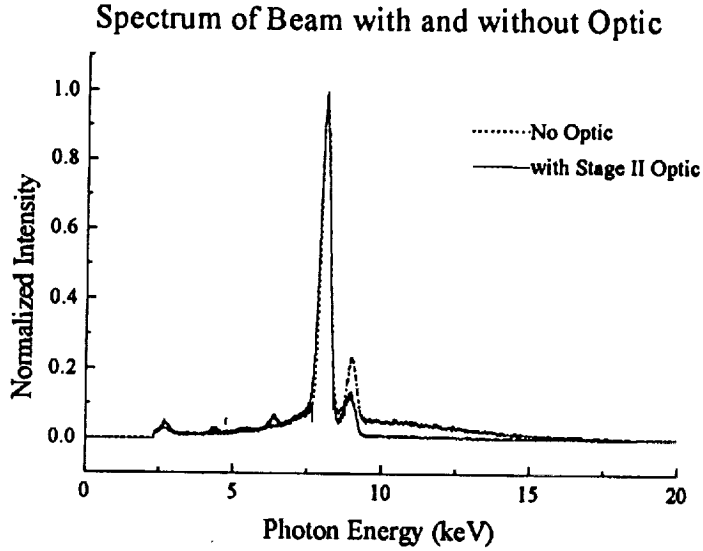

Figure 22. Energy spectra of x-rays from a bare Cu anode at 37.5 kV and after passing through the Stage II optic.

40.4% in other regions. After passing through the Stage II optic, the percentages are 63.2% Kα, 9.1% Kβ and 27.7% in other regions. Further filtering of the Cu Kβ line can be achieved by placing a thin Ni Foil at the output of the optic. The bare spectrum and the spectrum through the Stage II optic and a 8 μm Ni filter are shown in Fig. 23. With the Ni filter the percentages are 75.4% Kα, 1.9% Kβ and 22.7% in other regions. This is the condition used for most of our further measurements (it was later determined that more Ni, ~12μm, is necessary to produce a clean enough spectrum for crystallographic use).

A. Stage I Optic.

The Stage I optic was a collimating optic and can be used to provide flux gain in most parallel beam applications. A schematic representation for this system is shown in Fig. 24. The geometric properties of this optic are outlined in Table 1. In order to use this optic efficiently on the Rigaku RU-300 rotating anode source at the Biological Structure Laboratory at MSFC, a new beryllium window mount was designed that allows access within 25 mm of the center of the source and the shutter was held open to allow space for the optic.

Scanning the optic in a direction transverse to the axis of the optic gives an approximate gaussian intensity distribution. The Width of Field is defined as the FWHM of this distribution and describes the maximum diameter of a source over which the optic will collect efficiently. Similarly, scanning the optic in a direction parallel to the optic axis, the position of highest transmission is defined as the input focus distance of the optic and the full width at 3//4 of the maximum is defined as the Depth of Field. Fig. 25 shows the Width and Depth of Field for the System I optic. The measured Width of Field is 0.16 mm. The most optimum source for this optic would then be a 0.2 mm diameter circular source, but most rotating anode sources are line sources 10 times longer that wide, and when

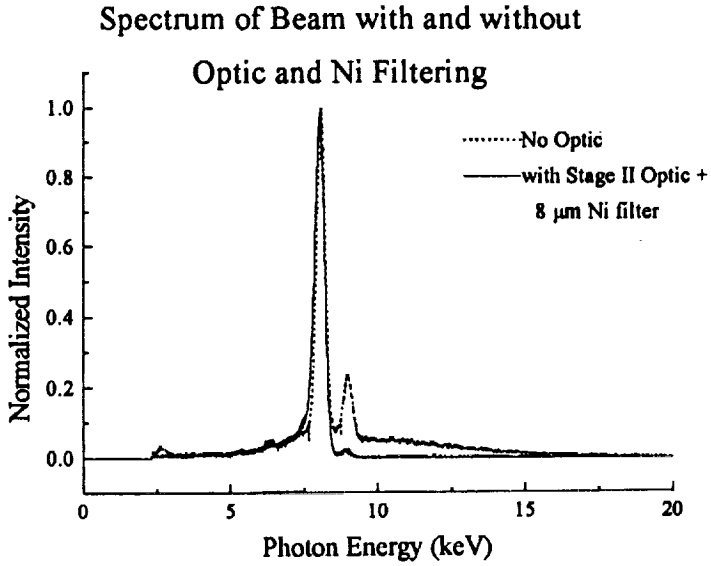

Figure 23. Energy spectra of x-rays from a bare Cu anode at 37.5 kV and after passing through the Stage II optic and a 8 μ m Ni filter.

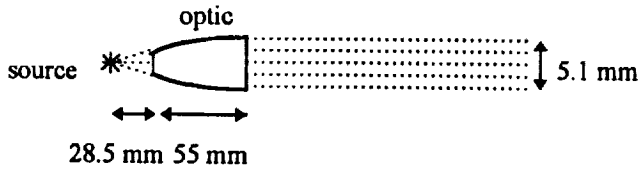

Figure 24. Schematic representation of the Stage I optic geometry.

Property	Stage I
output D (mm)	5.1
input d (mm)	3.2
length L (mm)	55
input focus length (mm)	28.5
input capture angle ω (rad)	0.11
transmission*	28.3 %

*Table 1. Geometric properties of the Stage I optic. * The transmission value was measured for Cu Kα with a 0.16 mm diameter source.*

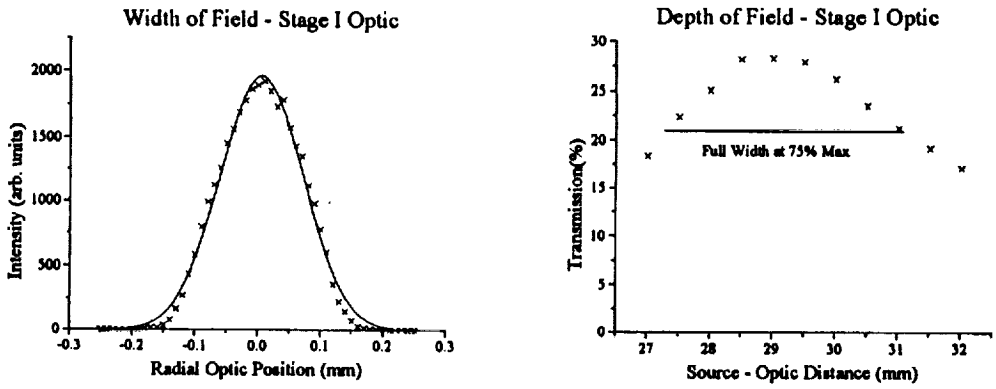

Figure 25. Scans defining the Width and Depth of Field for the Stage I optic.

viewed at a 6° take off angle appear square. Therefore, the appropriate rotating anode source for this optic would be one with a 0.2 x 2.0 mm spot size. The optic will collect efficiently over the entire depth of such a source, since the measured Depth of Field is 3.7 mm.

The rocking curve of a Si(400) Bragg reflection was used to measure the output divergence of the optic. The measured rocking curve is shown in Fig. 26. This scan contains components from both the Cu $K\alpha_1$ and the $K\alpha_2$ lines that are not resolved due to the divergence of the beam. The separation of the two lines is well known (20 eV corresponding to 0.98 degrees) and the $K\alpha_2$ line is exactly half the height of the $K\alpha 1$ line. The measured curve was poorly fit by assuming a combination of gaussian or a combination of lorentzian distributions but was successfully deconvoluted by using a special technique developed by Professor Catichia at the University at Albany (private communication). The resultant deconvoluted curve (fit by a gaussian to be consistent with other divergence measurements) is shown in Fig 27. As shown, the Stage I optic has an output divergence that is nearly gaussian in shape with a FWHM of approximately 3 mrad.

The Stage I optic was mounted to a Rigaku RU 300 rotating anode source with a 0.3 mm x 3.0 mm spot, operating at 2.8 kW. The optic was also mounted to a KEVEX sealed tube source with a 0.2 mm x 2.0 mm spot, operating at 40 W. In all cases, a 0.3 mm diameter collimator was used. This included the "standard" system, which was another Rigaku rotating anode with a 0.3 mm x 3.0 mm spot, operating at 2.8 kW, a graphite monochromator, and a source-crystal-distance of 250 mm. The estimated and measured gains for the Stage I optic are given in Table 2. The considerably larger measured gain compared to the expected gain may be due to the fact that the output beam of this optic is not uniform with a higher transmission through the center than the outer portions. A central

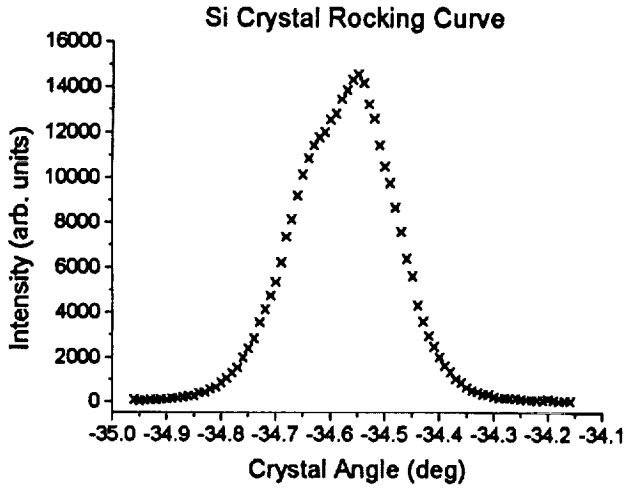

Figure 26. Silicon (400) rocking curve using the output of the Stage I optic.

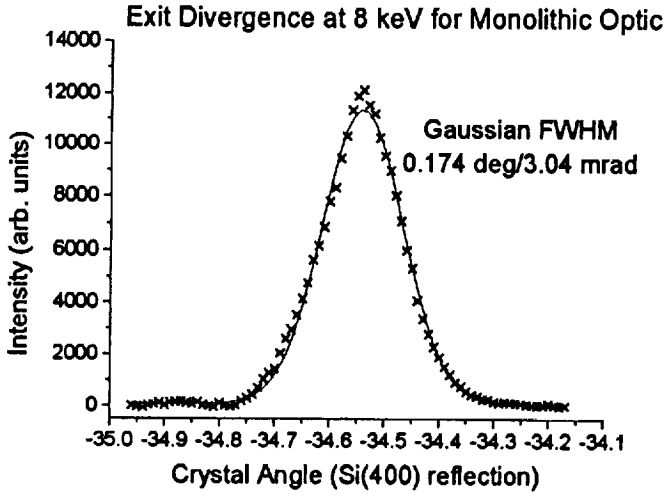

Figure 27. Deconvoluted Si (400) rocking curve and gaussian fit for the Stage I optic.

transmission of 35% as opposed to the whole optic value of 28.3% would provide an estimated gain of 3.2. The x-ray flux estimated for the sealed tube and the rotating anode systems when used with the Stage 1 optic are summarized in Table 3. The obvious question here is why is the estimated flux using the KEVEX sealed tube source, 28 times smaller than for using a rotating anode source, while the measured flux (from Table 2) is only 15 times smaller? This may be due to larger than assumed absorption in the rotating anode line source observed at 6^{o} or to the larger depth of the rotating anode source. The answer to this is not clear.

Diffraction patterns were taken with this optic on a Ragaku 300 rotating anode source coupled to a Seimens 3-axis goniometer and a multiwire area detector. An example of such a diffraction pattern for a lysozyme crystal is shown on Fig. 28. With this system, no apparent difference in diffraction image quality has been seen compared to the standard system (with graphite monochromator). Quantitative comparisons were not made because of the limited time available (the majority of available time was spent on study of the Stage II optics and the effect of beam convergence). With this source/optic combination a full diffraction data set for a 0.2 mm x 0.2 mm x 0.3 mm lysozyme crystal required 4 hours to collect. (Subsequently, a large number of high quality measurements have been made with this system for a variety of proteins).

B. Stage II Optic.

The Stage II optic has a slightly different geometry than the Stage I optic. The input characteristics are similar (albeit with a smaller capture angle, ω), but the output has a slight decrease in diameter, creating a slightly focused beam. A schematic representation of this optic is shown in Fig. 29 The geometric properties for this optic are given in Table 4. The Width and Depth of Field scans are shown on Fig. 30. With a Width of Field of 0.23 mm, a Depth of Field of 9.7

Source type and spot size	Estimated Gain with filtering	Measured Gain w/o filtering	Measured Gain adjusted to include filtering
Rotating anode, 0.3 mm x 3 mm	2.6	8.0	3.2
Sealed tube, 0.2 mm x 0.2 mm	0.10	0.55	0.22

Table 2. Gain estimates for the Stage I optic. Measured values are compared to the flux achieved with the "standard" rotating anode with a 0.3 mm x 3.0 mm spot and a graphite monochromator.

Source type, spot size and power applied	Number of Cu Kα photons/sec
Standard Rot. anode, 0.3 x 3, 2.8 kW	1.7×10^8
Rotating anode, 0.3 x 3, 5.4 kW	3.3×10^8
Rotating anode, 0.2 x 2, 3.2 kW	3.4×10^8
Kevex sealed tube, 0.2 x 0.2, 40 W	6.1×10^6
Variable focus, 0.204 mm dia, 408 W	6.5×10^7

Table 3. Estimated x-ray flux incident on a 0.3 mm diameter crystal using the Stage I optic and a variety of sources. Fluxes quoted assume that the optic is used in conjunction with a 40% filter to ensure spectral quality.

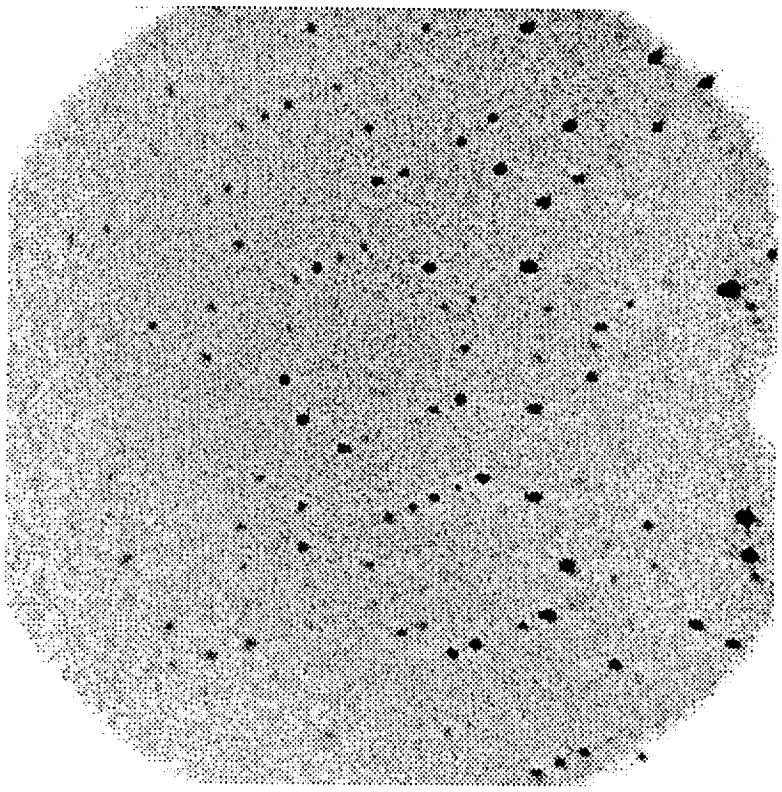

Figure 28. Diffraction image from a lysozyme crystal. The center of the detector is at 2Θ = 35°, and the image took 90 seconds to record. Similar images using the "standard" system can take as much as 20 minutes to record.

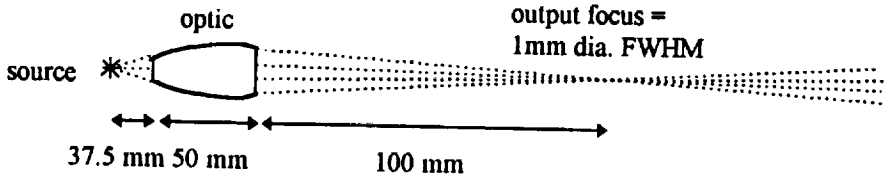

Figure 29. Schematic representation of the Stage II optic geometry.

Property	Stage II
output D (mm)	4.85
maximum diameter (mm)	5.1
input d (mm)	3.1
length L (mm)	50
input focus length (mm)	37.5
output focus length (mm)	100
input capture angle ω (rad)	.07
transmission	26.5 %

Table 4. Geometric properties of the Stage II optic. The transmission was measured for Cu Kα with a 0.16 mm diameter source.

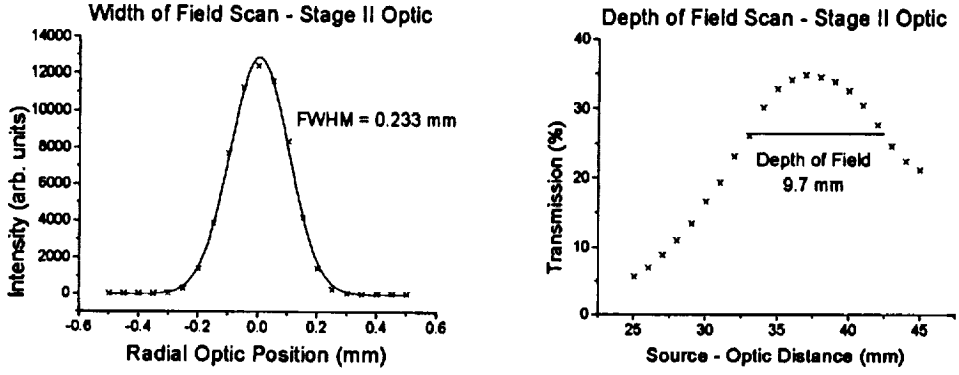

Figure 30. Width and Depth of Field scans for the Stage II optic.

mm and an input focal distance of 37.5 mm, this optic has a good fit to the Ragaku RU 300 rotating anode generator and can be used without modification of the beryllium window or shutter assembly. The only geometric drawback of this optic compared to the Stage I optic is that it has a significantly smaller (40% of Stage I) capture efficiency. The slightly focused output beam has a focal point 100 mm from the output of the optic. This was determined by scanning across the beam with a Lead edge. The results of this which show the focal distance as will as the width at the focus are shown in Fig. 31. An intensity map taken by scanning with a 0.25 mm pinhole at 100 mm from the optic is shown in Fig 32. The pinhole scan fits very well to a 2-D gaussian with a FWHM of 1 mm.

In order to determine the convergence angle of the beam, the rocking curve of a Si(400) reflection was measured and fit to a gaussian. The FWHM of the rocking curve was almost exactly 1 degree. Since it is so large, there is little aberration due to the convolution of the Cu $K\alpha_1$ and $K\alpha_2$ lines, so the deconvolution procedure used for the Stage I optic was not necessary, The scan and gaussian fit are shown in Fig. 33. The convergence angle becomes smaller once the beam is passed through a collimator, as is necessary for crystallographic studies to reduce background. The beam convergence through a 0.17 mm diameter collimator was measured as 0.52 degrees FWHM. Collimators up to 0.5 mm diameter yielded beams with similar convergence.

The Stage II optic was mounted to a Rigaku 300 rotating anode source and the beam intensity was measured through a 0.3 mm diameter collimator. As for the Stage I optic, measurements were performed without filtering and corrected for a 40% filter. The gain over the standard collimator/monochromator system is 28.9. The estimated x-ray flux using the Stage II optic for a variety of sources is given in Table 5. It is striking to see that the combination of the 40 W KEVEX source and the Stage II optic should provide nearly the same flux as that obtained from the

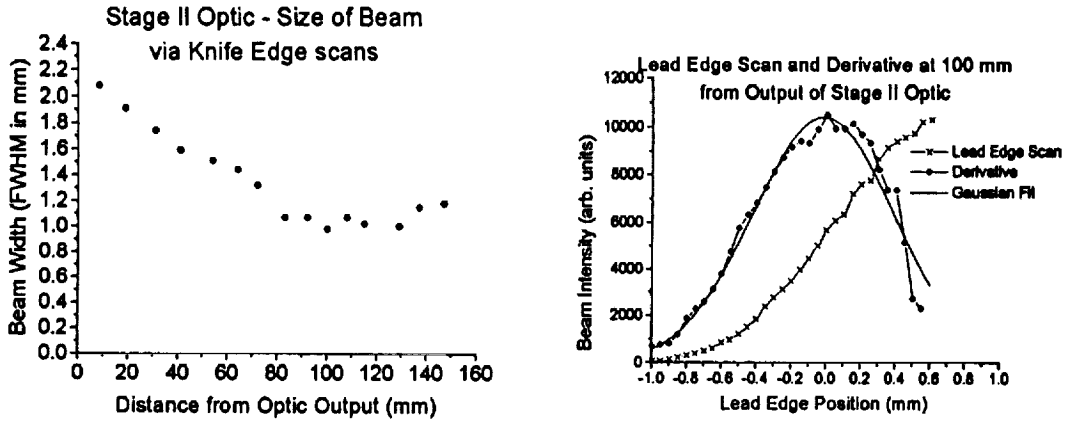

Figure 31. Beam width from the Stage II optic as determined by Lead edge scans.

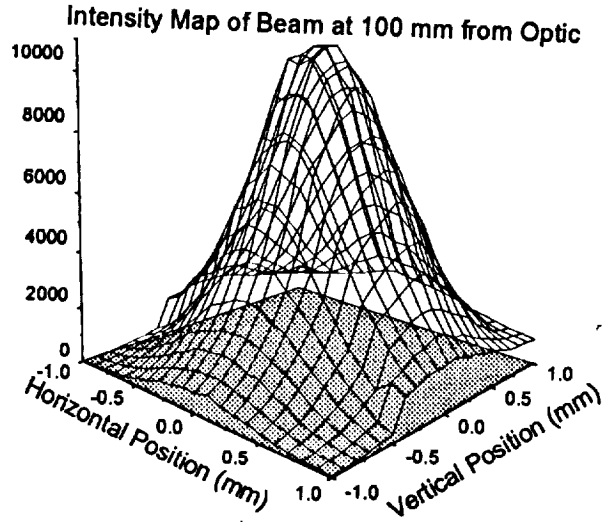

Figure 32. Pinhole scan at the focal point of the beam from the Stage II optic.

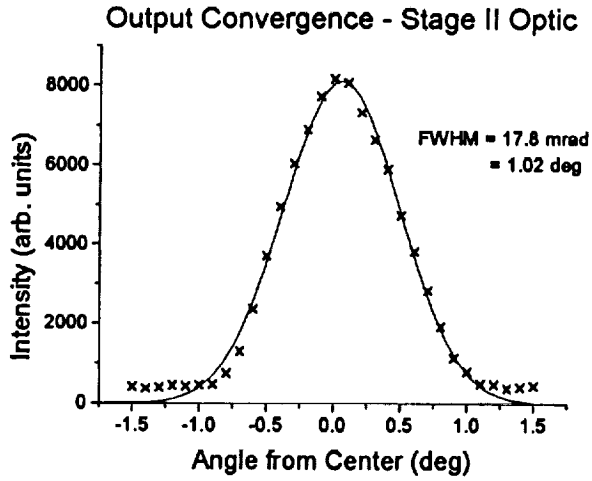

Figure 33. Rocking curve of a Si(400) reflection using the Stage II optic.

Source type, spot size and power applied	Number of Cu Kα photons/sec
Rotating anode, 0.3 x 3, 5.4 kW	3.7×10^9
Rotating anode, 0.2 x 2, 3.2 kW	3.0×10^9
Kevex sealed tube, 0.2 x 0.2, 40 W	5.7×10^7
Variable focus, 0.303 mm dia, 606 W	7.2×10^8

Table 5. Estimated flux incident on a 0.3 mm diameter crystal using the Stage II optic and a variety of sources. Fluxes quoted assume that the optic is used in conjunction with a 40% filter to ensure spectral quality.

standard 2.8 kW rotating anode generator with a graphite monochromator. Furthermore, with a water cooled, sealed tube source of appropriate spot size one could achieve an order of magnitude more flux than the standard system without the high cost and maintenance of a rotating anode. However, it is important to note that the intensity is not the only consideration. It remains to be discussed whether a 0.5 degree convergent beam will be useful for crystallography especially using current software analysis packages.

For a focusing system with a preset focusing angle and distance (as is the case for polycapillary optics), it is mechanically simpler to focus the beam on the crystal than on the detector. Doing so maximizes the intensity at the crystal but may have drawbacks with respect to diffraction spot size and cross-fire. It was not possible in the present study to investigate the possibility of focusing the beam on the detector because of restrictions on the source-crystal and the crystal-detector distances for the system used. The most significant effect of focusing the beam on the crystal in the tangential broadening of diffraction spots due to beam cross-fire. A sample diffraction image is shown in Fig. 34 for a lysozyme crystal taken with the Stage II optic and A Rigaku RAXIS II image plate detector. This image clearly shows the effect of the 0.5 degree convergent beam focused at the crystal position. It appears from Figure 34 b and c that the broadening effects high angle reflections more than low angle ones. This is consistent with a detailed analysis which has been carried out subsequent to the study covered in this report.

For this range of convergence, the resolution and point spread factor of the detector being used appears to make a significant difference. Using the Stage II optic and a Siemens multwire proportional detector, the broadening of spots is not apparent. An example of such a diffraction pattern is shown in Fig. 35. Indeed, except for the very much reduced exposure time, with this system, the diffraction patterns are indistinguishable from those obtained with the "standard" system if

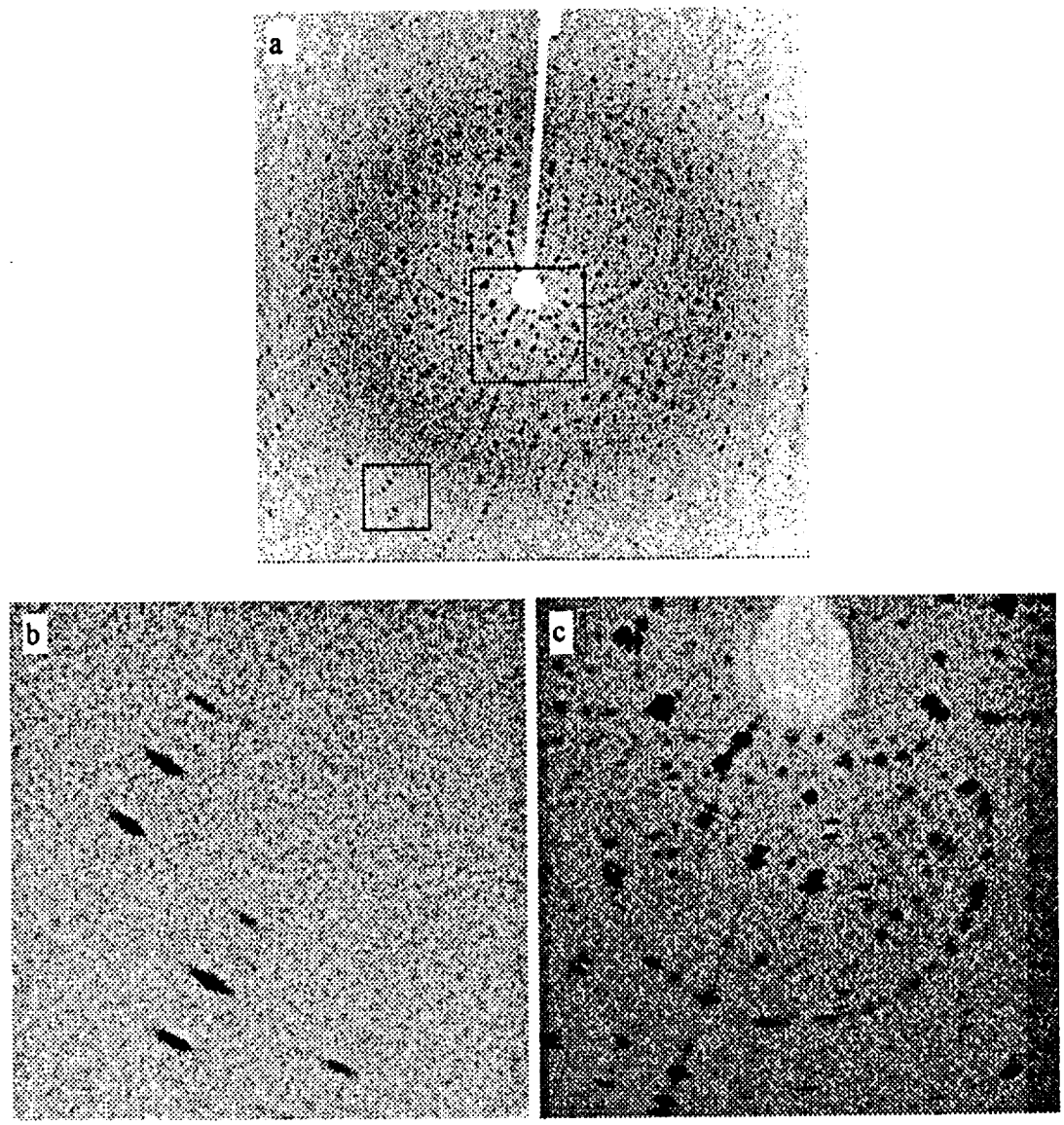

Figure 34. Still lysozyme diffraction images recorded on a Rigaku RAXIS II detector showing the tangential broadening of spots due to beam convergence.

the same detector is used. Also, if normal oscillation exposures are taken with the RAXIS II detector, the diffraction spots even at high angles become rounded and the problem of spot elongation does not appear to be so significant. The image shown on Fig 36 shows a 2 degree oscillation image that took only 20 seconds to acquire.

The obvious advantage of focusing the beam on the crystal compared to parallel beam crystallography is that the direct beam intensity is much higher. This has two important results: 1. The minimum size of useful crystals is smaller; and 2. The necessary exposure time is shorter. These are non-trivial benefits since two of the major difficulties in protein crystallography are growing large, high quality crystals and collecting data before radiation damage destroys the crystal quality. With respect to use of small (or thin) crystals, a 1 mm x 0.1 mm x 0.02 mm canine serum albumin crystal was successfully measured with the 0.3 mm collimated beam from the Stage II optic.

Full data sets were collected for lysozyme crystals using a Rigaku RU 300 rotating anode generator and a Rigaku RAXIS II detector with the Stage II optic and an 8 μm Ni filter (this arrangement gave 40 x intensity gain compared to the "standard" system). The native data file (to which the optic file will be compared) was taken with 1.75 degrees of oscillation per frame for 35 minutes each and 35 frames were collected. The optic data was taken with 2 degrees of oscillation per frame for 3 minutes each and 28 frames were collected. The agreement between the data sets was measured by the "merging R factor" which is a comparison of the scattering factors and intensities of the two data sets, and is given as a percentage difference. The merging factors are also quoted for a specific resolution; the R factors at resolution higher than 2 or 3 Angstroms quickly diverge for most crystals. For the optic data set at 2.5 Angstrom resolution, the merging R facto based on F^2 (the intensities) was 5.7% and the merging R factor based on F

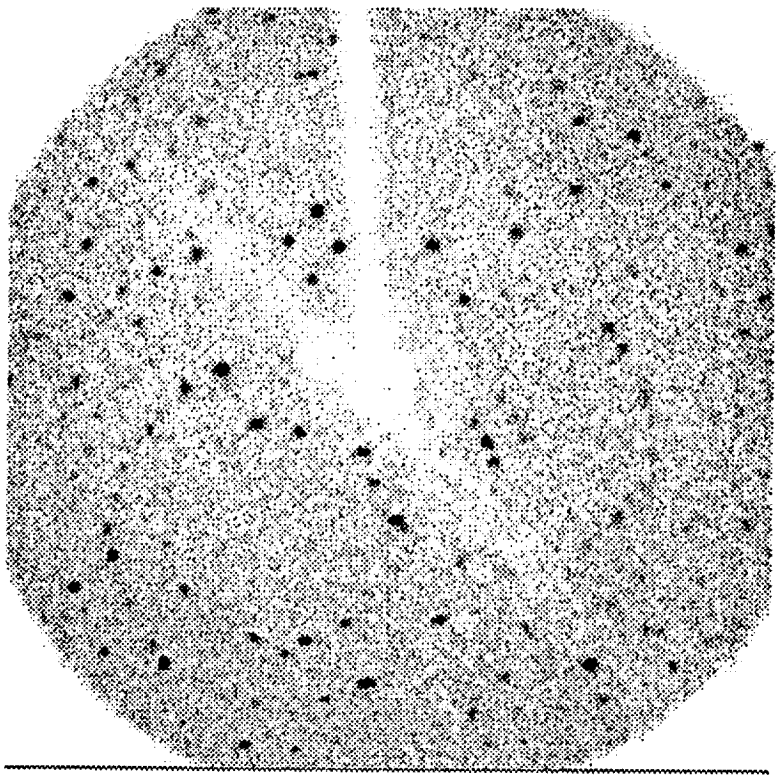

Figure 35. Still lysozyme diffraction image recorded on a Siemens multiwire proportional detector.

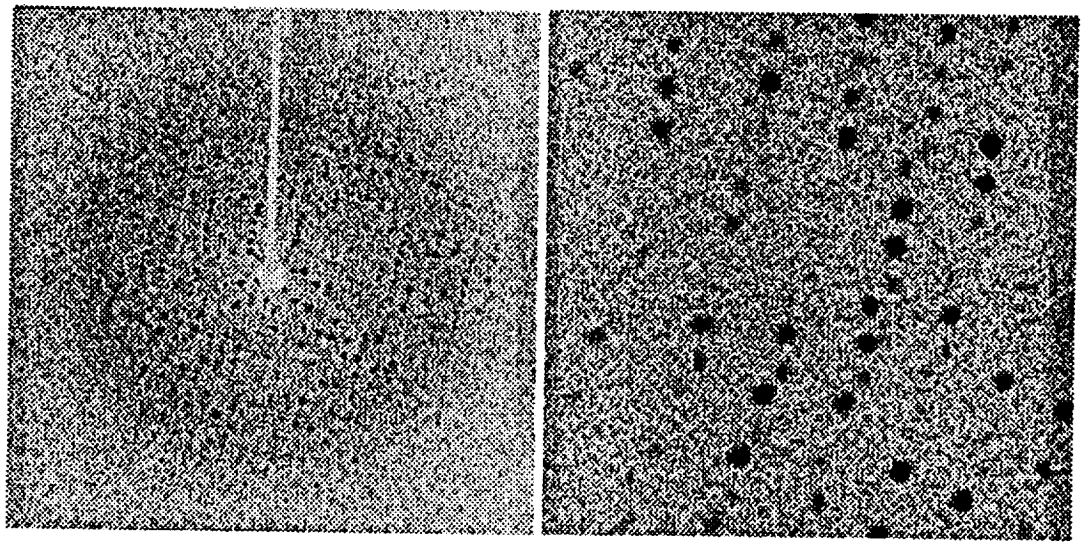

Figure 36. 2 degree oscillation lysozyme diffraction image recorded on a Rigaku RAXIS II detector. The magnified image is centered at approximately 3 Angstrom resolution.

(the scattering factors) was 4.0%. For protein crystallography, this is excellent agreement especially considering the filtering uncertainty and the fact that unmodified analysis software was used for both data sets. In practice, two data sets taken with the "standard" setup on two different crystal yield similar R factors.

This result shows that using a 0.5 degree convergent beam focused on the crystal is a feasible experimental technique, at least for medium unit cell size crystals and reasonably high resolution. Modification of current analysis software to account for the beam convergence may make high resolution or larger unit cell studies possible in the future. Such measurements may be especially useful for small crystals in order to help evaluate crystal growth techniques and in preparation for higher resolution Synchrotron based studies.

C. Stage III Optic

The Stage III optic is a highly focusing optic. The Width of Field and output focal spot sizes are small and the input and output focus distances are short. This means that the optic cannot be used with an unmodified rotating anode x-ray generator and that the output beam has a large convergence angle and is not suited for standard crystallography (ie; cannot be used with standard analysis software). However, the large output convergence angle means that a larger volume of reciprocal space is sampled in a single exposure and produces a dramatically increased intensity and a smaller spot size. The geometrical properties of the Stage III optic are shown in Table 6. The Width of Field scan for the Stage III optic is shown in Fig. 37 which shows a FWHM of 0.158 mm. With the Width of Field shown, this optic will collect 52% of the area of a 0.2 mm x 0.2 mm source and 30% of a 0.2 mm x 0.3 mm source. The most appropriate source for this optic would be a 0.205 mm diameter circular source, a good fit to the available KEVEX tube source.

Property	Stage III
output D (mm)	3.1
maximum diameter (mm)	5.1
input d (mm)	3.4
length L (mm)	31
input focus length (mm)	34 ± 2
output focus length (mm)	24 ± 2
input capture angle ω (rad)	0.1
output focusing angle (rad)	0.13
transmission* (%)	9 ± 2

*Table 6. Geometric properties of the Stage III optic. * The transmission was measured for Cu Kα with a 5 μ m diameter source.*

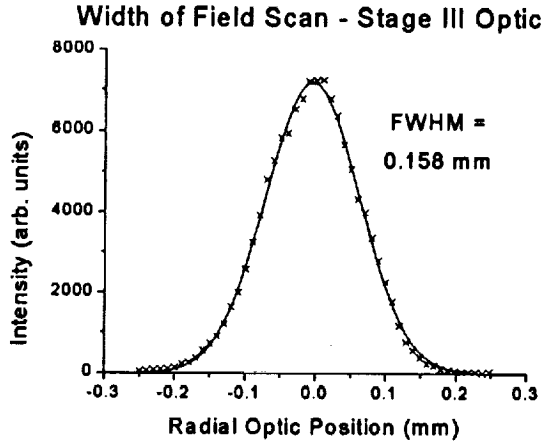

Figure 37. Width of Field scan for the Stage III optic.

The output beam is highly convergent. The focal point is 24 mm from the output of the optic and the focal spot size is 106 μm in diameter (0.1 mm). The output diameter of the optic is 3 mm, yielding a geometric convergence angle of 7.2 degrees. However, the optic does not transmit uniformly, thus the actual convergence profile of the beam is gaussian in nature and the FWHM is less than 7.2 degrees. The convergence angle was determined from two independent measurements; a pinhole scan directly at the output and measurements with an area sensitive detector far from the focal point. A Si rocking curve could not be measured because the detector available was much smaller than the total angle subtended by ant rocking curve and a Θ-2Θ stage was not available.

A pinhole of 0.17 mm diameter was scanned across the output of the optic in 0.15 mm steps. This scan with a gaussian fit is shown in Fig. 38. This result, together with the known 24 mm focal distance, gives a FWHM of 2.65 degrees. The full width of 2.5 mm at the base shows that x-rays with convergence up to 6.5 degrees is present. In order to vary the total convergence from this optic,and to cut off the most convergent x-rays, a series of apertures were used at the output of the optic. Measurements with four of these apertures are shown in Fig. 39. The FWHM measurements of the output beam convergence for the different apertures from the pinhole scans and from the area detector measurements are summarized in Table 7.

The intensity gain for the Stage III optic with the Rigaku RU 300 rotating anode generator (including an 8 μm filter) is 188. Even mounted to the 40 W KEVEX source, the beam is 17 times more intense than the "standard" rotating anode system. The estimated total flux for the Stage III optic with various sources is shown in Table 8. It must be stressed that the usefulness of the Stage III optic

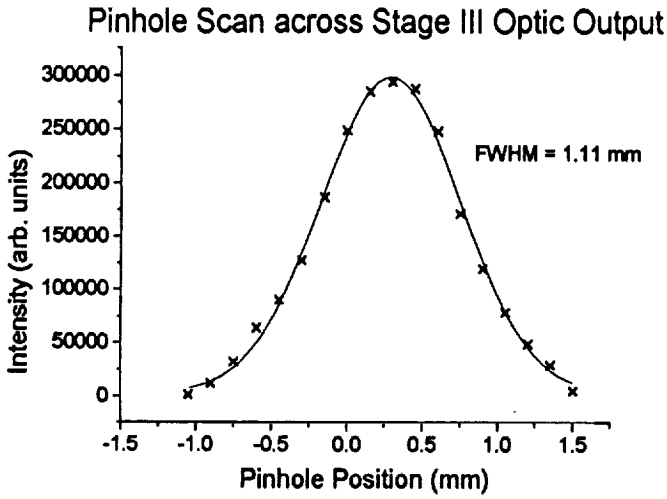

Figure 38. Relative intensity across the Stage III optic.

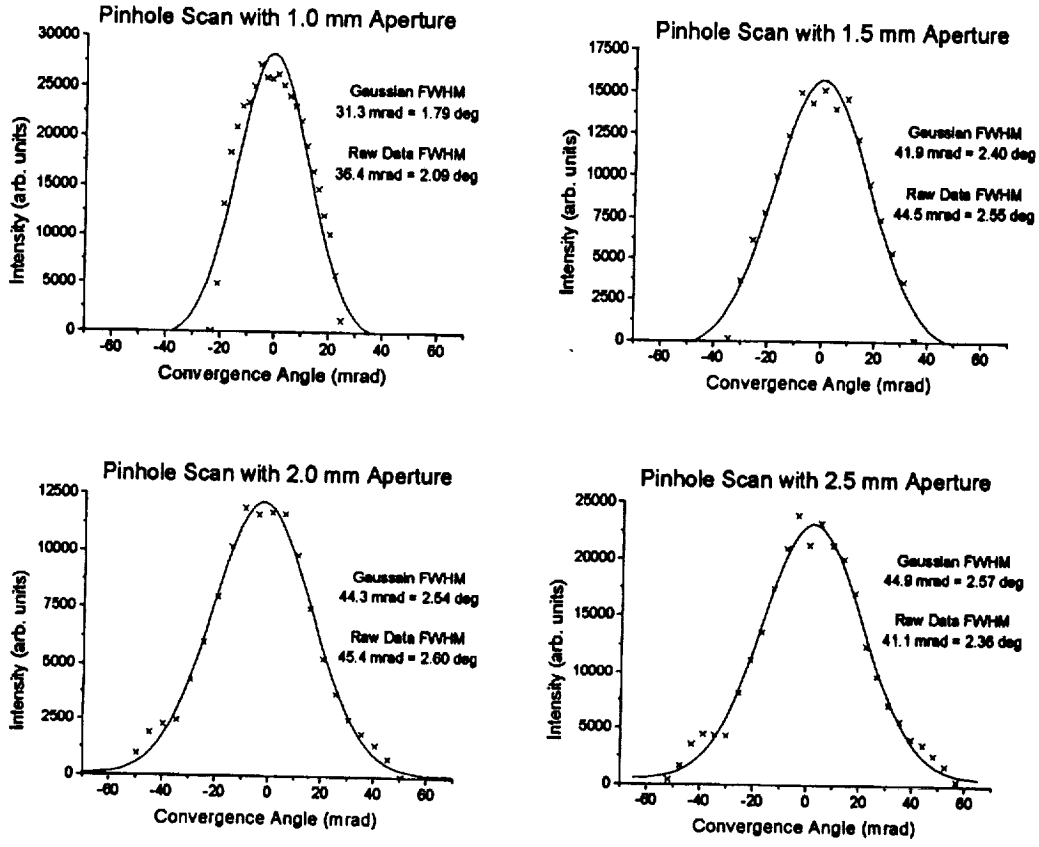

Figure 39. Convergence angle distributions from the Stage III optic with various diameter apertures over the output of the optic.

Aperture diameter	Pinhole Scans (raw data)	Area Detector Images (ave of horz & vert)
2.5 mm	2.36 deg FWHM	2.15 deg FWHM
2.0 mm	2.6	2.1
1.5 mm	2.55	2.1
1.0 mm	2.09	1.8
0.45 mm	N/A	0.83
0.17 mm	N/A	0.47

Table 7. Output convergence angles for the System III optic with various apertures at the output as determined by pinhole scans and area detector images.

Source type, spot size and power applied	Number of Cu Kα photons/sec
Rotating anode, 0.3 mm x 3 mm, 5.4 kW	2.4×10^{10}
Rotating anode, 0.2 mm x 2 mm, 3.2 kW	2.5×10^{10}
Kevex tube, 0.2 mm x 0.2 mm, 40 W	4.8×10^{8}
Variable focus, 0.205 mm diameter, 410 W	5.0×10^{9}

Table 8. Estimated x-ray flux incident on a 0.3 mm crystal from the Stage III optic and a variety of sources. Fluxes quoted assume that the optic is used with a 40% filter to ensure spectral purity.

is dependent on solving the problems associated with using such beams for structure determinations.

A photograph of the Stage III source-optic-crystal-detector system is shown on Fig. 40. To qualitatively illustrate the effect of increasing the convergence on diffraction spots, the detector was moved back to 300 mm from the crystal. Diffraction images were then taken for a lysozyme crystal with various apertures placed over the output of the optic. The change in spot elongation as a function of convergence angle is seen clearly in Fig. 41. With the Siemens multiwire detector in a normal position at 100 mm from the crystal and at $2\Theta = 0$, the edges of the detector are at approximately 3 Angstrom resolution. Even at that resolution, images with good statistics were recorded in 5 minute exposures using a 35 W KEVEX source. as shown in Fig 42. Given the convergence angles of the beam for the two images shown in Fig 42, full data sets with 50% redundancy and 0.1 degree overlap between frames can be collected with 30 and 80 frames respectively. At 5 minutes per frame this corresponds to full data sets in 2.5 and 6.7 hours with a 35 W source! If these values scale correctly and such an optic can be designed for use on a rotating anode source, a full data set to 3 Angstrom resolution using 2 degrees of convergence could be collected in approximately 6 minutes (neglecting readout time delays). Furthermore, because the focused spot sizes of highly convergent beams are so small (20 μm has been demonstrated for x-ray microfluorescence), crystals as small as 20-30 μm could be used, helping with one of the major bottlenecks of protein crystallography, large crystal growth. Conversely, for some applications (such as planetary landers or rovers or bore hole or remote locations, very small power sources (as low as 1 W) can be used. Realization of these possibilities will depend on development of appropriate analysis software.

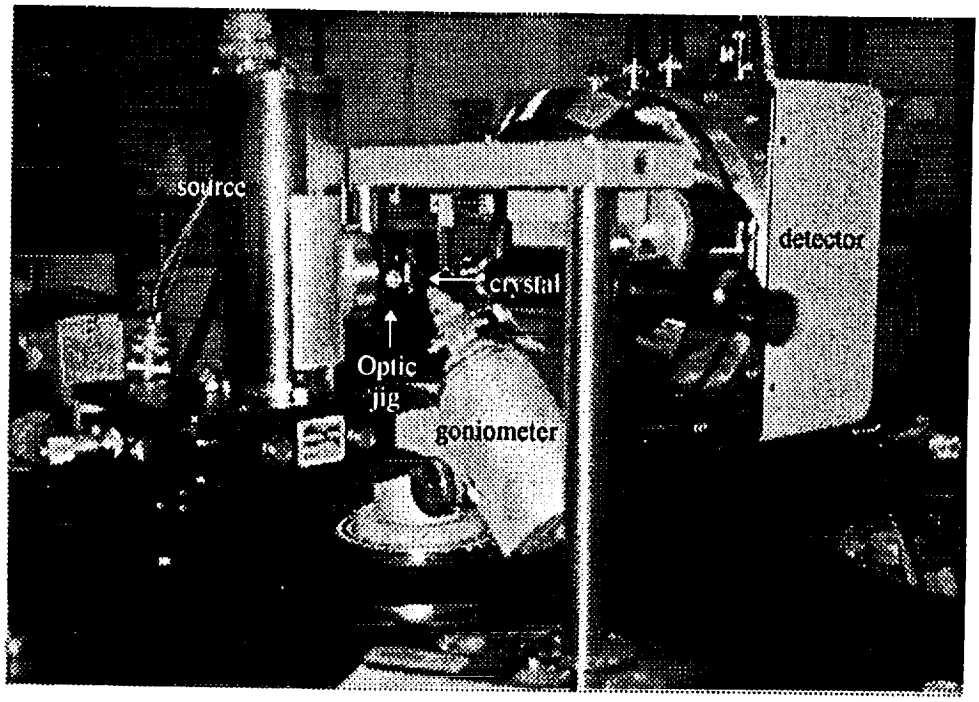

Figure 40. Photograph of the source-optic-goniometer-detector arrangement for the Stage III optic.

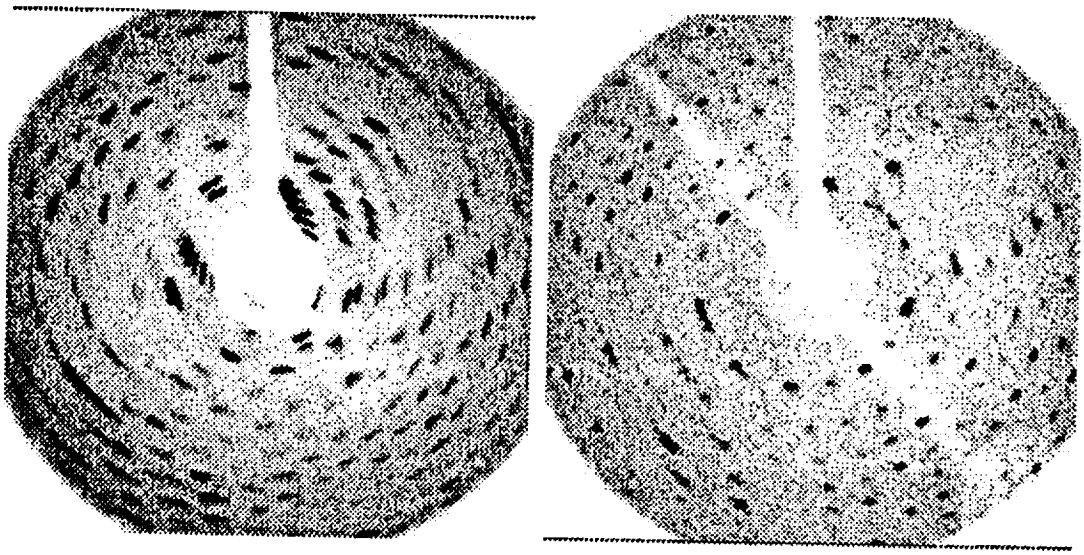

Figure 42. Still lysozyme diffraction images taken with the Kevex source/Stage III optic/Siemens detector system. The crystal-detector distance was 100 mm. Apertures placed at the output of the optic limited the beam convergence to 2.1 and 0.83 degrees respectively.

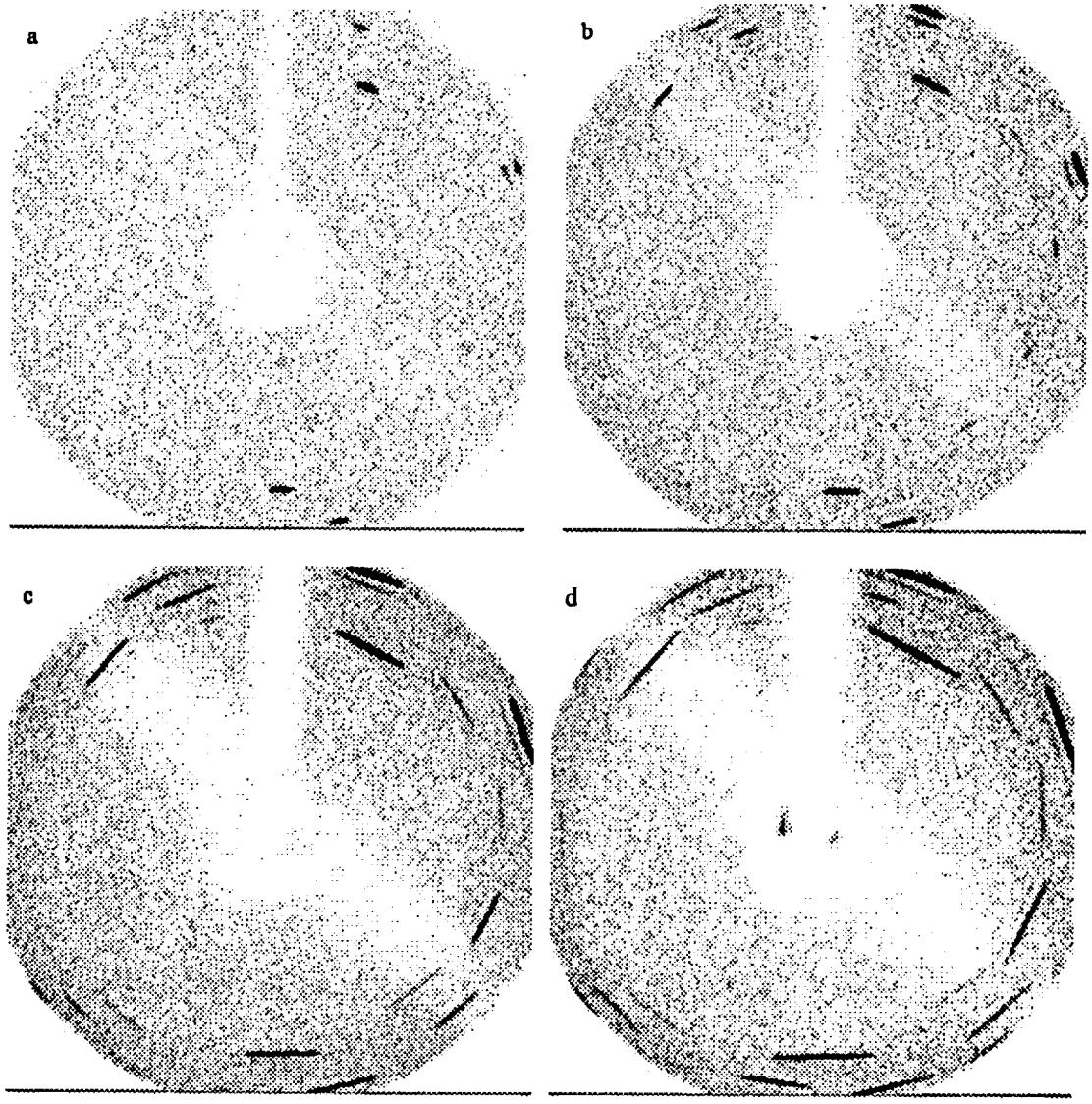

Figure 41. Still lysozyme diffraction images with varying convergence angles recorded on a Siemens multwire detector. The crystal-detector distance was increased to 300 mm for these images. Images a, v, c, and d correspond to 0.47, o.83, 1.80, and 2.10 degree convergence respectively.

Section IV. PRESENTATIONS AND PUBLICATIONS

A. Presentations:

J.B. Ullrich, I.Yu. Ponomarev. M.V. Gubarev, N. Gao, Q.-F. Xiao, and W.M. Gibson, "Development of Capillary Optics for X-Ray Diffraction Applications", invited paper, in X-Ray and UV Detectors, R.B. Hoover and M.W. Tate, eds., SPIE Annual Conf. San Diego, CA, July, 1994 (Published in SPIE Proceedings Vol. **2278** (1994).

B.K. Rath, D.C. Aloisi, D.H. Bilderback, N. Gao, W.M. Gibson, F.A. Hofmann, B.E. Homan, C.J. Jezewski, I.L. Klotzko, J.M. Mitchell, S.M. Owens, J.B. Ullrich, L. Wang, G.M. Wells, Q.-F. Xiao and C.A. MacDonald, "Effects of Intense X-ray Radiation of Polycapillary Fiber Performance" in X-Ray and Ultraviolet Sensors and Applications, R..B. Hoover and M.B. Williams, eds. SPIE Annual Conf. San Diego, AA, July 1995 (Published in SPIE Proceedings, vol. **2519**, 1995)

S.M. Owens, J.B. Ullrich, I.Yu. Ponomarev, D.C. Carter, R.C. Sisk, J.X. Ho, and W.M. Gibson, "Protein Crystal Structure Measurements Using Polycapillary X-Ray Optics", SPIE Annual Conf. Denver CO, August, 1996, (Published in SPIE Proceedings, Vol. **2859**, 1996))

J.B. Ullrich, S.M. Owens, Q.-F. Xiao, I.Yu. Ponomarev, D. Carter, R.C. Sisk, W.M. Gibson, "Convergent Beam Macromolecular Crystallography Using Polycapillary X-Ray Optics", poster presentation at the Joint American Crystallography Association and the International Crystallography Union (IUCr) Conference, Seattle Washington, Aug. 1996.

S.M. Owens, J.B. Ullrich, I.Yu. Ponomarev, W.-F. Xiao, D. Carter, R.C. Sisk, and W.M. Gibson, "X-Ray Optics for Macromolecular Crystallography", poster presentation at the Joint American Crystallography Association and the International Crystallography Union (IUCr) Conference, Seattle Washington, Aug. 1996.

S.M. Owens, C.A. MacDonald, D.C. Carter, J. Ruble, and W.M. Gibson, "X-Ray Diffraction with Polycapillary Optics", invited paper at Denver X-Ray Analysis Conference, Steamboat Springs, CO, August, 1997, (to be published in Conference Proceedings)

B. Publications:

Johannes B. Ullrich, "Studies of Monolithic Capillary Optics for Small Sample Crystallography", Ph.D. Thesis, University at Albany, State University of New York, May, 1995.

Scott M. Owens, "Development of Polycapillary X-Ray Optics for Macromolecular Crystallography", Ph.D. Thesis, University at Albany, State University of New York, May, 1997.

C.A. MacDonald, S. M. Owens, D.C. Carter, J. Ruble, and W.M. Gibson, "Convergent Beam X-Ray Diffraction Analysis ", (accepted for publication in Journal of X-Ray Crystallography, Jan. 1998)

Joseph X. Ho, Eddie H. Snell, R. Charles Sisk, John R. Ruble, Daniel C. Carter, Scott M. Owens and Walter M. Gibson, "Stationary Crystal Diffraction with a Monochromatic Convergent X-Ray Source and Application for Macromolecular Crystal Data Collection", *Acta Crystal.*, **D57**, 200-209 (1998)

Section V. PROJECT SUMMARY AND FUTURE PLANS

This project has demonstrated the feasibility of polycapillary x-ray optics to enhance data collection for macromolecular crystallography. A variety of optics have been studied, each with their own befits and limitations.

The Stage I optic provides a moderate gain in intensity over a simple collimator-monochromator system (from 3.2 to 5 times depending on the necessary level of spectral filtering). The beam characteristics (divergence, diameter and energy band width) are within the specifications required by most studies. One of the greatest benefits is that the $1/r^2$ dependence of the beam intensity is eliminated, allowing more flexibility in the experimental design. Closer coupling of the x-ray source and the optic than was possible with the rotating anode source available for this project can greatly increase the intensity and Bragg diffraction of the output beam with a flat crystal could improve the collimation and energy purity of the beam.

The Stage II optic provides more than an order of magnitude larger gain in intensity over the standard system when the crystal is placed at the focal position of the beam (from 27 to 60 times, depending on the filtering). Although the convergence is larger than usually encountered for focusing mirrors (0.52 degrees FWHM), the data quality still appears to be high for moderately sized unit cells at

medium to high resolution. The convergence angle causes diffraction spots to be elongated, with a larger effect at higher diffraction angles. If standard oscillation techniques are used, integrated diffraction spots are somewhat larger than normal, but this does not appear to pose a serious problem.

The State III optic provides yet another order of magnitude gain in direct beam intensity. Even with a low power (35 W) tube source, the flux this optic can place on a crystal has been measured to be nearly 20 times more than the standard rotating anode system. The beam, however is highly convergent making the diffraction pattern too streaky for analysis with standard software. Possibilities for development of appropriate and effective analysis software appears promising.

All three types of optics can be improved by higher brightness x-ray sources with small spot sizes (<40 μm diameter) and close access (~2 mm) to the source allowing a larger collection angle (up to 0.2 radians for Stage I optics and 0.5 radians for Stage II and Stage II optics). This work has stimulated development of x-ray sources so some of these benefits can be realized.

In summary, the use of polycapillary x-ray optics for macromolecular crystallography can have significant benefit. Through large increases in direct beam intensity, polycapillary optics can provide previously unheard of decreases in necessary exposure time in a laboratory setting. Highly convergent beam crystallography should prove to be a powerful new tool for crystallographic analysis allowing crystallographers to use crystals ten times smaller that are currently used, allowing data to be collected at a faster rate using simpler and less expensive sources.